

Article

A Practicable Measurement Strategy for Compliance Checking Number Concentrations of Airborne Nano- and Microscale Fibers

Asmus Meyer-Plath *^{id}, Daphne Bäger, Nico Dziurowitz, Doris Perseke, Barbara Katrin Simonow, Carmen Thim, Daniela Wenzlaff and Sabine Plitzko

Bundesanstalt für Arbeitsschutz und Arbeitsmedizin (BAuA), Nöldnerstr. 40-42, 10317 Berlin, Germany; baeger.daphne@baua.bund.de (D.B.); dziurowitz.nico@baua.bund.de (N.D.); perseke.doris@baua.bund.de (D.P.); bksimonow@gmail.com (B.K.S.); thim.carmen@baua.bund.de (C.T.); wenzlaff.daniela@baua.bund.de (D.W.); plitzko.sabine@baua.bund.de (S.P.)

* Correspondence: meyer-plath.asmus@baua.bund.de

Received: 1 October 2020; Accepted: 17 November 2020; Published: 20 November 2020



Abstract: Despite compelling reports on asbestos-like pathogenicity, regulatory bodies have been hesitant to implement fiber number-based exposure limits for biodurable nanoscale fibers. One reason has been the lack of a practicable strategy for assessing airborne fiber number concentrations. Here, a method is proposed, detailed and tested for compliance checking concentrations of airborne nano- and microscale fibers. It relies on Poisson statistical significance testing of the observed versus a predicted number of fibers on filters that have sampled a known volume of aerosol. The prediction is based on the exposure concentration to test. Analogous to the established counting rules for WHO-fibers, which use a phase contrast microscopy-related visibility criterion of 200 nm, the new method also introduces a cut-off diameter, now at 20 nm, which is motivated by toxicological findings on multi-walled carbon nanotubes. This cut-off already reduces the workload by a factor of 400 compared to that necessary for imaging, detecting and counting nanofibers down to 1 nm in diameter. Together with waiving any attempt to absolutely quantify fiber concentrations, a compliance check at the limit-of-detection results in an analytical workload that renders our new approach practicable. The proposed method was applied to compliance checking in 14 very different workplaces that handled or machined nanofiber-containing materials. It achieved detecting violations of the German benchmark exposure level of 10,000 nanofibers per cubic meter.

Keywords: nanofiber; aerosol; workplace exposure assessment; fiber number concentration limit; occupational health and safety

1. Introduction

Fibrous particles can induce long-term inflammation and disease if they are respired into the alveolar region of the lung and are neither dissolved in lung fluids nor removed by lung clearance mechanisms due to their fiber morphology. This epidemiologically substantiated observation has been formulated as the so-called fiber pathogenicity paradigm [1,2]. It states that sufficiently long and biodurable respirable fibrous objects exhibit carcinogenic potential in lung tissue.

In light of the history of asbestos and asbestos-related diseases [3], it is of utmost importance for human health to detect, assess and control excessive concentrations of respirable biopersistent airborne fibers. For such an assessment, several measurement strategies, categorization concepts and counting rules have been developed internationally, mainly focusing on the availability of analytical techniques and on the industrial relevance of fibers of toxicological concern.

An important fiber counting method was developed by the World Health Organization (WHO) [4]. Fibers matching the dimensions specified in this rule are colloquially called WHO-fibers. They exhibit—motivated by respirability—diameters smaller than $D_{\text{WHO}} := 3 \mu\text{m}$, their length must exceed $L_{\text{WHO}} := 5 \mu\text{m}$ and their aspect ratio (length to diameter) $L/D \geq 3$. A detail sometimes neglected is the so-called visibility criterion, $D_{\text{PCM}} = 200 \text{ nm}$, of the WHO rules, which corresponds to the visibility limit of asbestos and other mineral fibers in optical phase-contrast microscopy (PCM) and sets a lower limit on the diameter of fibers to be counted.

However, asbestos-like toxicity has also been reported for biodurable fibers thinner than 200 nm [5–8], including nanofibers below 100 nm [9,10]. For comparable exposure concentrations, it is mandatory to explicitly specify the minimum diameter of the fibers that were actually included in a count result [11]. Using the term WHO-analogue fibers for analyses including sub-200-nm-fibers can help in emphasizing such ensemble differences.

To indicate concentrations of fiber fractions properly, the symbol $\text{WHO}_{D_{\text{lower}}}$ will in the following denote the number of WHO-fibers with diameters between D_{lower} and 3000 nm. Standard WHO-fibers are thus denoted as WHO_{200} -fibers, whereas, e.g., WHO_{20} denotes WHO-analogue fibers in the range of 20–3000 nm.

1.1. Established Limits for WHO-Fibers

Many countries have established legally binding concentration limits like occupational exposure limits (OEL) for selected types of WHO_{200} -fibers. The GESTIS database gives an international overview on workplace shift-averaged (eight hours) and short-term OELs, e.g., for asbestos or mineral fibers (<https://www.dguv.de/ifa/gestis/gestis-internationale-grenzwerte-fuer-chemische-substanzen-limit-values-for-chemical-agents>). The eight-hour limits are generally set between 10,000–100,000 $\text{WHO}_{200}/\text{m}^3$ for asbestos, with limits sometimes higher for chrysotile than amphibole asbestos, and around 200,000–1,000,000 $\text{WHO}_{200}/\text{m}^3$ for minerals and vitreous wools and fibers.

The Netherlands implemented two different asbestos OEL values, depending on analysis technique [12]. For the same exposure risk level, the associated fiber concentrations are set a factor of two higher for transmission electron microscopy (TEM) than for PCM results, since electron microscopic techniques enable visualizing fibers around the PCM visibility limit of $D_{\text{PCM}} = 200 \text{ nm}$ with higher reliability than PCM.

In Germany, only fibers thicker than 200 nm are counted, and the implemented concentration levels vary between 1000 $\text{WHO}_{200}/\text{m}^3$ and 100,000 $\text{WHO}_{200}/\text{m}^3$, depending on risk level and protection objectives. The German Technical Rule for Hazardous Substances TRGS 910 [13] for carcinogenic fibers distinguishes acceptance and tolerance concentrations of 10,000 $\text{WHO}_{200}/\text{m}^3$ and 100,000 $\text{WHO}_{200}/\text{m}^3$, which are related to 4 : 10,000 and 4 : 1000 fiber-induced cancer cases per worker life, respectively, using asbestos exposure-risk relations. A concentration below the clearance level of 1000 $\text{WHO}_{200}/\text{m}^3$ is mandatory before lifting protective measures on asbestos-contaminated buildings. These concentration ranges may be considered relevant also for pathogenic WHO-analogue fibers.

1.2. Established Limits for WHO-Analogue Fibers

Various toxicological studies suggest that assessing and limiting exposure concentrations of WHO-analogue fiber fractions is necessary. The authors who first introduced the fiber pathogenicity paradigm, Stanton et al., had already reported pathogenic effects of thin fibers, now sometimes called Stanton fibers, that were longer than 8 μm and thinner than 250 nm and found a strong correlation between tumor incidence and fiber number dose [14,15]. The French Agency for Environmental and Occupational Health Safety (ANSES) recommended “given the carcinogenic potential” to include thin asbestos fibers when determining dust levels in workplaces with TEM [16]. Toxicological concerns on biodurable nanofibers, especially carbon nanotubes (CNTs), have also motivated the inclusion of fiber fractions thinner than 200 nm into concentration measurements [5,7].

Meanwhile, several research projects and authors, as well as national standards and government advisory bodies, have recommended limits for nanofiber concentrations [13,17–20].

The National Institute for Occupational Safety and Health (NIOSH) of the United States, for instance, has published a (recommended) exposure level (REL) for the specific class of carbon nanotubes and carbon nanofibers (CNFs). At workplaces with potential exposures to CNTs and CNFs, the eight-hour average concentration of respirable elemental carbon is recommended to be kept below $1 \mu\text{g}/\text{m}^3$ [21]. Since other sources of elemental carbon in a workplace can interfere with the determination of CNTs and CNFs exposures, other analytical techniques such as TEM could assist in characterizing exposures by visualizing particle and fibrous morphologies [22]. The REL of $1 \mu\text{g}/\text{m}^3$ corresponds to the current analytical limit of elemental carbon quantification [21]. However, since this REL is not a fiber number but a mass concentration limit, it circumvents the problem of categorizing complex fiber morphologies as countable fibers or uncountable agglomerates and has the drawback of not allowing to identify correlations between toxicological effects and fiber number dose. In addition, even an analytical limit of $1 \mu\text{g}/\text{m}^3$ is about two to three orders of magnitude too insensitive to allow the detection of 10,000 individual toxicologically relevant nanofibers per cubic meter. Even if just 1 % of the nanofiber mass was aerosolized as individual WHO-analogue fibers, the sensitivity would be insufficient since $100,000 \text{ F}/\text{m}^3$ graphitic fibers of $15 \mu\text{m}$ length, 60 nm diameter and a density of $1.8\text{--}2.2 \text{ g}/\text{cm}^3$ would exhibit about $0.01 \mu\text{g}/\text{m}^3$. Currently, MWCNTs with diameters of 37 nm and above are considered carcinogenic [7].

The British Standards Institution [20] proposed a legally non-binding benchmark concentration for insoluble fibrous nanomaterials of $10,000 \text{ fibers}/\text{m}^3$ to be assessed by scanning EM (SEM) or TEM.

The German Committee on Hazardous Substances (AGS) prepared the German Technical Rule TRGS 527 “Activities with nanomaterials”, which was published recently by the German government [13]. The rule implements a benchmark concentration for the exposure to fibrous nanomaterials at workplaces

“For biopersistent fibrous nanomaterials with a length exceeding $5 \mu\text{m}$, a diameter below $3 \mu\text{m}$ and a length/diameter ratio exceeding 3:1, a concentration of below $10,000 \text{ fibers}/\text{m}^3$ should be ensured in the air at the workplace [13].”

The term nanomaterial here refers to the proposed EU definition [10], which includes nanofibers down to 1 nm and also thinner single-walled CNTs (SWCNTs). Since the definition comprises materials with a certain number fraction of nanoscale particles and fibers, consequently, microscale fibers may be present in an EU nanomaterial. The German value can thus be interpreted to correspond to $10,000 \text{ WHO}_1/\text{m}^3$, including SWCNTs. In contrast to the German and other asbestos OELs, this benchmark value is not health-based, since epidemiology-based exposure–risk relations are missing for nanofibers.

1.3. Guidelines for Determining WHO-Fiber Concentrations

Reproducible visualization, recognition, categorization, identification and counting of fibrous morphologies require detailed technical guidelines that specify how to achieve reliable imaging, identification of material composition, categorization of complex objects etc.

WHO-fiber measurement guidelines established on national levels aim at determining airborne fiber concentrations for consumer and occupational health and safety regulations. The majority were designed for asbestos and other mineral and vitreous fibers, including NIOSH Method 7400 and 7402 [23,24], VDI Guideline 3492 [25] and DGUV Information 213–546 [26]. They are based on the WHO_{200} counting rule and, generally, the 200 nm PCM visibility criterion to maintain epidemiological comparability of contemporary data to historic reports on fiber concentrations independent of the achievable microscopic resolution.

In Germany, for monitoring asbestos concentrations at workplaces, the technical rules for hazardous substances TRGS 402 [27], 519 [28] and 517 [29] apply the measurement strategy of the

DGUV Information 213–546 [26]. The latter requires the collection of respirable fibers on filters and the analysis of filter areas of up to 0.5 m² to detect up to 50 WHO₂₀₀-fibers, whichever occurs first. The DGUV protocol aims at an analytical sensitivity, defined in Appendix A.2, of 3338 WHO₂₀₀/m³ to quantify concentrations above 10,000 WHO₂₀₀/m³. The German asbestos clearance level below 1000 WHO₂₀₀/m³ is tested by following the VDI Guideline 3492 [25].

1.4. Development of WHO-Analogue Fiber Guidelines

For WHO₂₀₀-fibers, reliable visualization and recognition of their morphology is achievable at microscopic resolutions of about 100–200 nm, see Section 2.4.1. At such low resolutions, the analytical effort required for mapping and analyzing a filter area of 0.5 mm² is well manageable. For thinner WHO-analogue fibers, higher microscopic resolutions than 200 nm are required. However, the attempt to quantify thinner fibers with methods that were implemented for WHO₂₀₀-fibers can, especially for nanofibers, result in excessive analytical workload, if only the image resolution is increased, see Section 2.5. Therefore, nanofiber-adapted assessment concepts are necessary.

In the following, we propose such a strategy for assessing airborne concentrations of micro- and nanoscale fibers. This approach to reducing the workload is schematized in Table 1. Similar to established methods for WHO₂₀₀-fibers, we aim at detecting fibers after flow-controlled sampling on filters by microscopic analysis of finite filter areas. A first workload reduction is achieved by implementing a lower limit on fiber diameter. Such a cut-off is already in use in established counting rules for WHO₂₀₀-fibers: Fibers thinner than 200 nm are ignored.

Table 1. Workload reduction approach of the proposed compliance check strategy in estimated in workload units relative to the workload for WHO-fiber quantification.

Quantifying WHO ₂₀₀ -Fiber Concentrations	Inclusion of Nanofibers	Quantifying WHO ₁ -Fiber Concentrations	Exclusion of Uncritical Diameters ¹	Quantifying WHO ₂₀ -Fiber Concentrations	Waiver of Quantification ²	Compliance Checking WHO ₂₀ -Fiber Concentrations
Workload 1	$\frac{(200 \text{ nm})^2 / (1 \text{ nm})^2}{\times 40,000}$	Workload 40,000	$\frac{(1 \text{ nm})^2 / (20 \text{ nm})^2}{\times 1 / 400}$	Workload 100	$\frac{3 \text{ WHO}_{20} / 15 \text{ WHO}_{20}}{\times 3 / 15}$	Workload 20

¹ See Section 2.5.1.; ² See Section 2.7.3.

For nanoscale fibers, careful selection of this cut-off diameter is essential to reduce the analytical workload without ignoring potentially pathogenic fiber fractions. In Section 2.5.1, our choice of cut-off diameter of 20 nm is motivated in more detail. A second workload reduction can be achieved by waiving the aim to absolutely quantify fiber concentrations. Instead, we propose to check compliance of a workplace concentration with an exposure limit by estimating an upper limit on the true concentration, see Section 2.7.3. This is achieved by so-called null hypothesis testing.

For comparison, a first, rough estimate for a concentration from a Poisson-statistical interpretation of a fiber counting experiment requires observing about 15 fibers, whereas an upper limit on the true concentration can be estimated with a confidence level of 95 % from observing zero fibers, when 2.996 ≈ 3 was expected at the exposure limit concentration. A threshold of 15 fibers is suggested here, since the relative size of the probability interval [L_G; H_S] exceeds 100 % for less than 15 fibers cf. Table A2 in Appendix D.4.

2. Methodology

This section describes in detail the methodology underlying the proposed measurement strategy, including experimental aspects of sampling, imaging, categorization and quantification, as well as the statistical null hypothesis concept for compliance testing.

2.1. Measurement Outline

Table 2 outlines the workflow of the proposed measurement strategy. It also refers to the sections of this paper that describe further methodical details.

Table 2. General workflow of the measurement strategy.

Measurement Strategy Component	Section
1. Collect information on the handled or released product fiber	
1.1 SEM analysis to determine morphological characteristics and minimum diameter	Section 2.6.1
1.2 EDS, Raman and/or FTIR analysis to determine elemental and chemical composition	Section 2.6.3
2. Collect information on the workplace	
2.1. Relevant exposure limits	Section 1
2.2. Characteristics and duration of work task and ambient dust level	Section 2.2
2.3. Estimate the highest permissible specific air volume q_V	Section 2.3.2
3. Perform workplace aerosol sampling	Section 2.3
4. Select SEM imaging conditions	
4.1. Imaging resolution	Section 2.4
4.2. Online or offline analysis	Section 2.8
5. Visual filter inspection, fiber recognition, categorization, identification and counting	Section 2.6
6. Compliance checking following the detailed analysis workflow	Section 2.9
7. Measurement documentation and result reporting	

2.2. Analytical Requirements and Experimental Constraints

Determining the concentration of a specific fraction of airborne fibers is a demanding task. It requires a series of experimental and analytical steps that depend on several on-site conditions and experimental parameters.

- On-site conditions
 - Characteristics of emission events: Continuous or transient, localized or long-term
 - Monitoring conditions: Source distribution, site ventilation and ambient dustiness
 - Fiber-to-dust ratio: Probability of fiber concealment by overlaying dust particles
- Experimental and analytical parameters
 - Air sampling parameters: Flow rate, duration, proximity to emission sources
 - Capture efficiencies of collecting devices
 - Microscopic imaging resolution
 - Material composition distinction capability
 - Fiber morphology and material categorization reliability
 - Required confidence level

Some of these analytical requirements are universal in the sense that they are independent of fiber dimension. Universal analytical details require no nano-specific adaptation. For instance, the task of recognizing fibers on sharp microscopic images via their morphology is independent of fiber diameter, whereas the requirements for sharp imaging, individual fiber material analysis, as well as aerosol distribution and collection dynamics, depend both on fiber dimensions and composition. Only visualized and identified product fiber fractions will affect the resulting fiber concentration.

2.3. Airborne Fiber Sampling

The proposed measurement strategy applies sampling of airborne dust by filtration on membrane filters. The requirements on filters and sampling conditions are discussed below.

2.3.1. Filtration Materials

Imaging and counting of sampled fibers requires filter substrates that allow reliable recognition of fiber morphologies by means of microscopic imaging. Unless a filter is dissolved or dry-etched prior to analysis, it must not be composed of fibrous structures that might prevent recognition of the fibers under study, but rather of a porous membrane. Established asbestos and mineral fiber concentration methods use foamy cellulose ester membranes or porous polymer films of typically less than 20% porosity. A smooth surface between pores can help in discriminating fibers from the filter. Membrane porosities around 10% should be preferred, since the larger contiguous area between pores facilitates tracking a fiber's path.

Nuclear track-etched pore filters made from polycarbonate (PC) exhibit smooth surfaces and generally round pores. Using track-etched membranes of poor surface quality and with many oblique-angle pores should be avoided. Sputter coating the polymer with noble metals like gold, palladium or iridium provides electrically conductive surfaces of small grain-size that allow high-resolution electron scanning microscopic analysis of nanoscale objects.

For WHO₂₀₀-fibers, typically track-etched pore filters of 800 nm pore diameter are used. Filtering airborne nanoscale fibers may suggest the use of significantly smaller pore sizes to increase the filtration efficiency, as PC membranes with pores down to 50 nm diameter are commercially available. However, unless a very thin and mechanically sensitive membrane is used, at the same porosity, smaller pores can drastically enhance the pressure drop over the filter and limit the achievable airflow. For example, an airflow of 4 L/min through a PC membrane of 25 mm diameter, 10 % porosity, with pores of 250 nm diameter and a film thickness of 12 μm causes a pressure drop of 350 kPa. In our experience, many standard air sampling pumps for asbestos measurement do not exhibit the necessary flow-versus-pressure performance to maintain desired sampling flows in the multiple-liters-per-minute range with the high pressure drops caused by small filter diameter, low porosity, small pores and/or high film thickness.

The choice of pore size is therefore a trade-off between fiber deposition efficiency and achievable airflow. The task of counting WHO-analogue nanofibers, i.e., fibers longer than 5 μm, should admit using larger pores since inertial filter impaction and filter pore-edge interception probability tend to increase with fiber length and airflow rate.

Another lower constraint on pore diameter of track-etched membranes results from the requirement of unambiguously localizing a fiber's position. This is possible by recognizing constellations of random pore patterns in the vicinity of the fiber. To also enable filter orientation in optical microscopes, we recommend using filters with pores of at least 400 nm diameter. As a benefit of such post-imaging localizability of fibers, fiber material analysis becomes possible by correlative microscopic techniques using electron microscopy, energy-dispersive and Raman spectroscopy, see Section 3.6.

Typical filter areas to be analyzed for the presence of fibers amount to, e.g., 0.5 m² for quantifying occupational exposures in the order of 10,000 WHO₂₀₀/m² [26]. Since gravimetric dust quantification, which requires high filter loading and larger filter area, is not combinable with fiber quantification, the filter diameter can be reduced from the 37 mm of the German PGP-FAP sampling head to, e.g., 25 mm of the standard asbestos filter heads or even 13 mm, still providing more than 100 times the required area to be analyzed, see <https://www.gsa-messgeraete.de/PGP-FAP-adapter-universal-sampler-fibre-plastics-cylinder-supporting-sieve>.

2.3.2. Filter Sampling Constraints

The achievable fiber deposition densities on a filter are subject to several constraints. The higher the density, the smaller the area to analyze for an exposure limit compliance check, the lower the visualization workload at a given microscopic resolution. It is, therefore, desirable to increase the specific air volume $q_V = V_o/A_o$, i.e., the total sampled volume V_o per open filter area A_o . The total collected volume $V_o = \int_0^\tau \Phi(t) dt$ depends on the sampling duration τ and airflow $\Phi(t)$; for constant

flow $V_o = \Phi \cdot \tau$. For a clamped filter membrane of diameter d and clamping of width c , the open filter area is $A_o = \pi/4 \cdot d_o^2$ with effective diameter $d_o = d - 2c$.

The practically achievable specific air volume $\rho_V(\Phi; \tau; d_o)$ is constraint by the following aspects:

1. The sampling duration τ must be adapted to characterize brief or transient emission processes and short-term or longer work shifts. If durations are enforced to be short, higher flows will be favored to keep the filter area to analyze small.
2. The acceptable sampling flow Φ range is generally constraint by the required filter face velocity range that ensures effective fiber filtration by interception and inertial impaction. Additionally, the filter pressure drop and the pump performance profile, as well as dust pre-separation requirements by means of vertical elutriation may limit the accessible flow range.
3. Especially in dusty sampling environments, the specific air volume ρ_V may need to be adapted to the ratio of the ambient dust concentration n_{AD} to the targeted fiber concentration n_{EL} . Overloading filters with particles that may conceal sampled fibers and prevent recognizing a fiber or tracking its complete length must be avoided, since this would reduce the recognition probability of (long) fibers. Practical experience, test measurements and online-detection techniques like aerosol spectrometers or condensation particle counters may help to estimate airborne dust concentrations and to adapt sampling parameters accordingly. For completely unknown ambient dust levels, different specific air volumes should be collected in parallel to obtain analyzable samples.
4. Fibers traversing or being trapped inside pores are lost for analysis. The fiber deposition efficiency η_{dep} of the filter at the chosen flow rate must therefore be known or estimated since only fibers that can be visualized on the filter can be categorized and counted, cf. Section 2.3.1.

As Appendix B shows in detail, it is important to avoid any *overestimation* of the filter deposition efficiency η_{dep} and the flow Φ as well as *underestimation* of the open filter area by filter deposition studies, applying careful flow calibration and mechanically reliable filter clamping.

2.4. Quantification of Sampled Fibers

Quantification of airborne fiber concentration requires collection, imaging, recognition, morphology characterization, categorization, identification, counting and, finally, normalization to the analyzed air volume. Besides methodological flaws in selecting a suitable sampling strategy and sampling position at a worksite, all these steps are possible sources of systematic and statistical error.

2.4.1. Digital Imaging Resolution and Pixel Size

Contemporary optical, Raman and electron transmission or scanning microscopes use digital cameras or scanning techniques to provide pixelated image data. The microscopic visibility of particles and fibers in pixelated microscope images is primarily constraint by the achieved physical microscopic resolution r and, secondarily, by the lateral extension of the acquired image pixels s , called pixel size. If the pixel size is chosen to be larger than the physical resolution, $r < s$, the effectively usable digital image information will be reduced to a resolution of s by the spatial averaging of a sharp image. Meanwhile, a pixel size smaller than the resolution, $s < r$, corresponds to the digitization of an unsharp image and is generally data inefficient, since no significant additional information is acquired.

For the subsequent discussion on the required digital image information content, we therefore assume the pixel size s to be equal to or exceed the achieved microscopic resolution r

$$r \leq s \quad (1)$$

In this way, pixel size becomes a very convenient parameter to control image acquisition at resolutions necessary for recognition of relevant structures. It is better adapted to our problem than the traditionally used image magnification factor M , which is meaningless without specifying the total image size in number of pixels. If not specified by the microscope control software, the size s of square

pixels can be calculated in nanometers for a microscopy image of $P_x \cdot P_y$ pixels with $P_x \geq P_y$ from the 5×4 -inch-Polaroid-image-related magnification factor M

$$s = \frac{127,000,000 \text{ nm}}{M \cdot P_x} . \quad (2)$$

2.4.2. Digitized Fiber Recognition Requirements

For morphology assessment and categorization, the shape of individual fibers must be reliably recognizable. In digital, pixelated images, this recognition step relies on identifying a chain of grey-level-correlated pixels that must exhibit significant contrast to filter (or particle) background pixels. The image contrast results from a combination of the microscopic resolution and the material contrast, which depends on the microscopic technique used.

Any image resolution worse than a fiber's diameter reduces the perceivable contrast by blurring. For visualizing a fiber, the image resolution r and pixel size s must not exceed the fiber diameter D

$$r \leq s \leq D \quad (3)$$

For reliable visualization, a resolution of $r \leq D/2$, whereas for diameter determination, a resolution of $r \leq D/4$ is recommended. Thus, the thinner a fiber, the higher the required imaging resolution and the more pixel data are to be generated per analyzed filter area A . As a consequence, the number of image pixels $P_x \cdot P_y$ to be acquired increases quadratically with decreasing pixel size s

$$A = s^2 \cdot P_x \cdot P_y \quad (4)$$

2.4.3. Measurability of Fiber Diameter, Length and Aspect Ratio

For categorizing a fiber according to the WHO or WHO-analogue fiber criterion, its relevant morphological fiber features length L and diameter D must be determined pairwise to be able to calculate the aspect ratio AR . Such pairwise measuring, in principle, requires the fiber to be fully contained in a microscope image. Since the criteria only set upper or lower limits on diameter, length and aspect ratio, some fibers can be categorized as WHO-analogue fibers even if they are not fully contained in a microscope image, provided

$$L > 3D > 5 \mu\text{m} \text{ and } D_{\text{crit}} \leq D \leq 3 \mu\text{m}, \quad (5)$$

with D_{crit} being the cut-off diameter for nanofibers, e.g., 20 nm, as introduced below.

Diameter determination requires calculating the average of the measured diameters at at least three different positions along the fiber. For WHO categorization purposes, the diameter requires to be accurate only to a certain level. Firstly, to decide whether a fiber is thinner than $3 \mu\text{m}$ is easily achievable at the microscopic level. Secondly, whether an aspect ratio exceeds $L/D > 3$ must be decided only for fibers with $D > 5 \mu\text{m}/3$. Otherwise, the length criterion dominates. Thirdly, analytically more demanding is to decide whether a fiber is thicker than the lower visibility or the cut-off diameter D_{crit} of Section 2.5.2. However, for fiber counting alone, high-accuracy diameter measurement is generally not required, cf. Equation (3). It is even counter-productive for fiber categorization, since high diameter accuracy limits the offline measureable aspect ratio, see below.

For length determination of bent or curled fibers, the so-called rectified length along the fiber's path must be determined. It requires to be able to reliably recognize the course of a fiber, even across fiber crossings. Image analysis software may help to obtain reliable results.

For a fiber in a microscope image that is shorter than $5 \mu\text{m}$, direct WHO categorization is not possible if that fiber is not fully contained in the frame. During online filter analysis, the image frame will either be interactively repositioned to follow the course of the fiber and determine its length, or,

if the fiber’s visibility can be maintained, the image magnification will be reduced to image a larger filter area.

In the case of offline image analysis, cf. Section 2.8, the same position-calibrated filter area must be imaged a second time to include neighboring image frames to measure the full length of the fiber of interest. It is, therefore, instructive to estimate the fiber containment probability. The expectation value for the length of randomly placed and randomly oriented straight fibers that are fully contained in an image frame of $P_x \cdot P_y$ pixels at a pixel size s is

$$\langle L \rangle = \frac{1}{3} s \cdot \sqrt{P_x \cdot P_y} \tag{6}$$

and their aspect ratio AR is

$$\langle AR \rangle = \frac{\langle L \rangle}{D} = \frac{1}{3} \cdot \frac{1}{m} \cdot \sqrt{P_x \cdot P_y} . \tag{7}$$

For different image resolutions and pixel sizes, Table 3 lists calculated expectation values for aspect ratio and length. Images large enough to fully contain fibers longer than $5 \mu\text{m}$ with fair probability should be larger than $\sqrt{P_x \cdot P_y} \geq 3/s \cdot L_{\text{WHO}}$, i.e., $17 \times 13 \mu\text{m}^2$ for $P_x/P_y = 4/3$. For the fiber toxicology-related cut-off diameter $D_{\text{crit}} = 20 \text{ nm}$ of our approach, see Section 2.5.2, and the associated pixel resolution of about $r = s = 10 \text{ nm}$ required for reliable visualization of such thin fibers, it is recommended to acquire images with significantly more than 1700×1300 pixel each.

Table 3. Calculated expectation values for aspect ratio and length of randomly placed and randomly oriented straight fibers that are fully contained in an image frame of $P_x \cdot P_y$ pixels at a pixel size s . Lengths below the WHO cut-off length of $5 \mu\text{m}$ are marked in gray.

Image Data Pixels	Expected Length $\langle L \rangle/s$	Pixel Size s	Image Size	Expected Length $\langle L \rangle$
3400 × 2600	991 pixel	5.0 nm	} 17.0 × 13.0 μm ²	5.0 μm
2048 × 1566	597 pixel	8.3 nm		
1700 × 1300	496 pixel	10.0 nm		
1280 × 960	313 pixel {	5.0 nm	6.4 × 4.8 μm ²	1.6 μm
		8.3 nm	10.6 × 8.0 μm ²	2.6 μm
		10.0 nm	12.8 × 9.6 μm ²	3.1 μm
2560 × 1920	739 pixel {	5.0 nm	12.8 × 9.6 μm ²	3.7 μm
		8.3 nm	21.2 × 15.9 μm ²	6.1 μm
		10.0 nm	25.6 × 19.2 μm ²	7.4 μm
5120 × 3840	1478 pixel {	5.0 nm	25.6 × 19.2 μm ²	7.4 μm
		8.3 nm	42.5 × 31.9 μm ²	12.3 μm
		10.0 nm	51.2 × 38.4 μm ²	14.8 μm

Flexible fibers may be deposited on filters in a bent or curled shape. This will enhance the fraction of contained fibers longer than the WHO limit.

2.5. Fiber Diameter-Related Workload

Controlling an exposure limit of $n_{EL} = 10,000 \text{ WHO}_{200}/\text{m}^2$ for WHO_{200} -fibers thicker than 200 nm according to the German “Method for determining concentrations of respirable inorganic fibers in working areas” [26] requires complete analysis of a filter area $A = 0.5 \text{ mm}^2$ or counting of at least 50 WHO_{200} -fibers. The quadratic scaling law of Equation (4) is exemplified in Table 4 for exposure limit control on a such an area of $A = 0.5 \text{ mm}^2$. With a pixel size of $s = 100 \text{ nm}$ required to reliably visualize fibers of diameter $D = 200 \text{ nm}$ and above, imaging of such an area is achievable with little effort.

Table 4. Number of pixels and images to acquire for analyzing 0.5 mm² or 0.5 mm²/5 = 0.1 mm² filter area. Image numbers of currently hardly or not yet manageable workload are marked in grey.

Pixel Size <i>s</i>	Filter Area to Analyze: 0.5 mm ²			Filter Area to Analyze: 0.1 mm ²		
	Pixels to Acquire	Images à 1280 × 960	Images à 5120 × 3840	Pixels to Acquire	Images à 1280 × 960	Images à 5120 × 3840
	$P_x \cdot P_y$	Pixel	Pixel	$P_x \cdot P_y$	Pixel	Pixel
100 nm	0.05×10^9	41	3	0.01×10^9	8	1
20 nm	1.3×10^9	651	41	0.16×10^9	130	8
10 nm	5.0×10^9	4069	254	1.0×10^9	814	51
8.3 nm	7.3×10^9	5907	369	1.5×10^9	1181	74
5.0 nm	20×10^9	16,276	1017	4.0×10^9	3255	203
2.5 nm	80×10^9	65,104	4069	16×10^9	13,021	814
1.0 nm	500×10^9	406,901	25,431	100×10^9	81,380	5086

However, for nanoscale fibers of about $D = 20$ nm in diameter, on a filter area of $A = 0.5$ mm², reliable visualization becomes a gargantuan task, requiring the acquisition and analysis of $5 \cdot 10^9$ pixels at a pixel resolution of 10 nm. For nanofibers of $D \leq 10$ nm, at least $20 \cdot 10^9$ pixels are required to image and evaluate the area A , which appears practically impossible with contemporary technology. A motivation for limiting the fiber diameter to image will be given in Section 2.5.1, whereas a desirable reduction of filter area to evaluate motivates waiving the determination of absolute fiber numbers in Section 2.7.1.

2.5.1. Workload Reduction by Introducing a Cut-Off Diameter

With the aim of reducing the analysis effort to a practicable amount, we propose using the so-called fiber rigidity hypothesis [6,8,30,31]. It toxicologically motivates ignoring a specific fraction of thin fibers and thus permits reducing the resolution of image acquisition. The rigidity hypothesis extends the fiber pathogenicity paradigm by imposing that only fibers that exceed a specific threshold of flexural rigidity show fiber-like toxicity. Fibers of lower rigidity, i.e., higher flexibility, are assumed to spontaneously curl or bend under forces applied by cells or tissue and to not behave in a fiber-like manner, but rather a more granular material-like manner [32]. Analogous to the fiber pathogenicity paradigm, the extended paradigm also ignores the specific material composition and considers only properties assumed to be relevant for inhalative toxicity. Physically, flexural rigidity R is a product of flexural, or bending modulus E_f and second moment of a fiber’s axial cross-section area I_a

$$R = E_f \cdot I_a \tag{8}$$

For isotropic and homogeneous materials, the flexural and tensile, or Young’s, modulus are identical. For a fiber of diameter D , the second moment of axial area I_a is

$$I_a = \iint_{\| \begin{pmatrix} x \\ y \end{pmatrix} \| \leq D} y^2 dx dy = \frac{\pi}{64} D^4. \tag{9}$$

Flexural rigidity thus scales proportionally with the modulus and to the fourth power of diameter. As a consequence, the effects of fiber diameter on rigidity easily dominate over small modulus differences. For materials of similar flexural modulus, a “critical rigidity” value R_{crit} , which separates flexible from rigid, carcinogenic fibers, can be simplified to a “critical diameter” D_{crit} . Thus, for materials of identical composition and microstructure, the introduction of a toxicologically motivated cut-off value on fiber diameter appears justified.

The analytical consequences of imposing such a rigidity-motivated cut-off diameter are similar to that of the PCM visibility-motivated diameter limit of $D_{PCM} = 200$ nm implemented in international

and national counting rules: Both allow a reduction in the number of pixels to image and search for toxicologically relevant or PCM-visible fibers, respectively.

2.5.2. Critical Flexural Rigidity to Derive a Cut-Off Diameter

Any toxicologically motivated cut-off diameter must—in principle—be chosen according to the alveolar response to fibers of known flexural rigidity. Currently, however, the level of critical rigidity causing fiber-like toxicity of biodurable fibers has not been determined exactly. Since no epidemiological data are available on nanoscale fiber toxicology, the data most relevant for human toxicology have been obtained by *intrapertoneal* (*i.p.*) testing. Most *i.p.* test results on nanofibers of known diameter and composition are available for multi-walled carbon nanotubes (MWCNTs) Figure 7.2 in Ref. [8]. Rittinghausen et al. reported a positive, fiber-like *i.p.* test result for the—so far—thinnest MWCNT material of 37 nm mean diameter [7].

Carbon nanotubes (CNTs) became famous for being very high modulus materials compared to other nano- and microscale fibers Table 7.3 in Ref. [8]. However, depending on the synthesis method and the measurement technique, MWCNT can show a rather broad variation of elastic modulus values of 1200–20 GPa Table 1 in [30]. The higher values resulting from single-walled CNTs and (early) arc synthesis, the lower ones from (later) mass-produced MWCNTs by catalytical chemical vapor deposition (cCVD).

For MWCNTs, Broßell et al. proposed a first estimate of the critical rigidity of about $R_{\text{crit}} = 0.5 \cdot 10^{-19} \text{ N} \cdot \text{m}^2$, based on 37–44 nm (mean 40 nm) diameter and 36–1000 GPa (mean 550 GPa) elastic modulus [8]. Even if the *i.p.*-tested MWCNTs with a mean diameter of 37 nm had a very low modulus of 50 GPa, the resulting rigidity of about $R = 5 \cdot 10^{-21} \text{ N} \cdot \text{m}^2$ would correspond to that of nanofibers of just $D = 20 \text{ nm}$ and a modulus of about $E_f = 550 \text{ GPa}$, cf. Equation (9).

It therefore appears justified to propose a toxicologically motivated critical diameter of $D_{\text{crit}} = 20 \text{ nm}$ that separates rigid from flexible high-modulus fibers. More flexible, low-modulus fibers should show larger critical diameters. With respect to a critical rigidity estimated from *i.p.* test data on 40 nm fibers, a $D_{\text{crit}} = 20 \text{ nm}$ includes a safety margin of about $(40/20)^4 = 16$ for inaccurately known modulus values and/or missing *i.p.* test data on thinner fibers. Deriving a more reliable R_{crit} or D_{crit} value will also require careful characterization of thinner *i.p.* test batches using—currently missing—validated rigidity measurement techniques.

Reliable imaging of fibers with $D_{\text{crit}} = 20 \text{ nm}$ requires microscopic resolutions of at least 10–20 nm, which are also still achievable for most low-end scanning electron microscopes. For reasons of the broad applicability of the proposed nanofiber measurement strategy, a technical argument can thus also motivate a diameter cut in this range.

The proposed critical fiber diameter of $D_{\text{crit}} = 20 \text{ nm}$ is one order of magnitude below the current visibility criterion of WHO₂₀₀-fiber counting rules of $D_{\text{PCM}} = 200 \text{ nm}$. If it is applied with the aim of nanofiber-including fiber concentration determination, the analytical workload will increase by a factor of $(D_{\text{PCM}}/D_{\text{crit}})^2 = 100$, cf. Table 1. Smaller cut-off values tend to result in unmanageably large pixel numbers, cf. Table 4.

2.6. Fiber Number Determination

To check compliance with a limit for WHO-fiber number concentration, the EM images of the filter samples must be evaluated visually or with the help of image analysis software. Recognized particles are to be dimensionally measured, morphologically categorized, substance identified to arise at a count of potentially biopersistent WHO-fibers. By analogy with the WHO asbestos counting rules, a distinction is made between respirable and not-respirable objects. Moreover, only fiber-containing objects will be analyzed in detail.

2.6.1. Morphological Categorization of Respirable Fiber-Containing Objects

Air and liquid suspensions of fibers generally not only contain individual and sometimes self-crossing fibers, but also loosely tangled or tightly bundled fibers, and, last but not least, agglomerates comprising many entangled fibers. The measured suspension state therefore partially depends on preparation and handling processes, partially on mechanical and surface-chemical properties of the fibers [33]. Any fiber number concentration that is determined by analyzing sampled aerosols or suspensions therefore only reflects the state of a specific fiber ensemble at the time of sampling. In addition, determined concentrations will be highly dependent on the details of categorizing these various morphologies. Therefore, detailed decision rules and well-trained personnel are necessary to arrive at comparable analysis results.

The case of bundled fibers illustrates the requirements for a categorization guideline: Both chrysotile asbestos and SWCNTs are nanoscale fibers that form multi-fibril bundles already during synthesis. Any resulting fiber concentration will thus depend on whether the fibrillary structure of bundles can be resolved microscopically, what fiber and bundle diameters are to be included in the analysis, and whether bundles are counted as one object or as individual fibrils.

The measurement strategy defines five morphological classes for the categorization of fiber-containing objects that are considered respirable ($D < 3 \mu\text{m}$), cf. Table 5. Only fiber-shaped ($L/D \geq 3$), and not the not fiber-shaped ($L/D < 3$), objects contribute to the counting result. The fiber-shaped objects are individual fibers or are composed of individual fibers to form bundled, tangled or agglomerated fibers. All countable fiber-shaped objects with length $L \geq 5 \mu\text{m}$ contribute to the number of WHO-analogue fibers in the sample, see Section 2.6.2.

2.6.2. Fiber Counting Rules

All objects that can be assigned to one of the categories listed in Table 5 must be analyzed further using a set of counting rules that are defined in the following and are illustrated in Table 6. For an assignment of recognized fiber-containing objects to one to the categories in Table 5, it is necessary to pairwise determine their length and diameter as described in Section 2.4.3.

In case individual fibers are visible within a fiber agglomerate or fiber bundle, they are to be individually measured, categorized and counted, provided they can be traced from tail to tail. If this is not feasible, the object is considered an agglomerate and its total length and mean diameter are used for its categorization. A bundle with no individually recognizable constituent fibers is to be treated as an individual fiber.

A fiber that has no tail contained in the EM image frame is not counted, since its tails would be further analyzed when appearing in neighboring images. For a fiber that shows one end while the other protrudes the image frame border, its visible length is measured. If the visible length exceeds , the fiber is weighted as a half WHO-analogue fiber. If the protruding fiber is shorter than $5 \mu\text{m}$, the offline evaluation approach requires the filter sample to be re-inserted into the SEM to determine the true total length of this fiber in a second imaging run to distinguish “half” WHO-analogue fibers from short, not counted fibers. For this purpose, the positions of image frame and the fibers of interest must be documented during the first run and be retrievable during the second run for accurate SEM stage positioning. During an online EM evaluation, the image frame can be adjusted interactively along a fiber’s path to determine its full length. Table 6 schematically exemplifies some important counting cases.

Table 5. Categories for categorizing respirable particles according to morphology, exemplified by example images. The length of the scale bar is 2 μm .

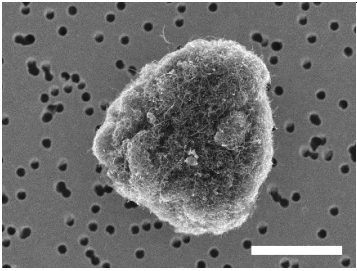
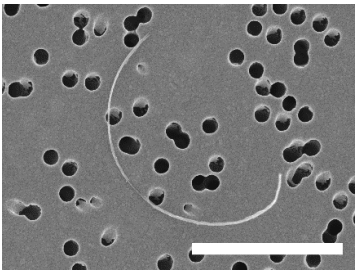
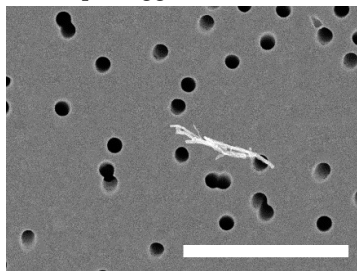
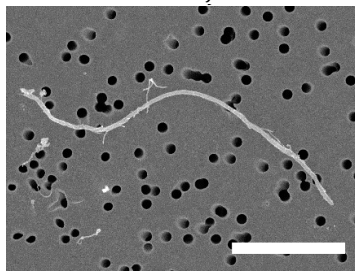
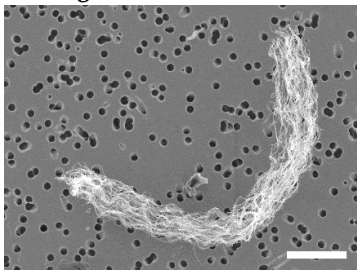
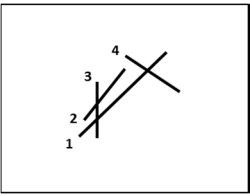
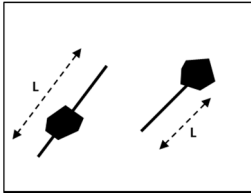
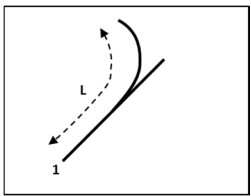
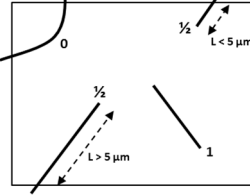
Objects Not to Be Counted as WHO-Analogue Fibers	
	Not fiber-shaped agglomerates with $L/D < 3$
	Short individual fibers with $L < 5 \mu\text{m}$ and $L/D > 3$
	Short fiber-shaped agglomerates with $L < 5 \mu\text{m}$ and $L/D > 3$
Objects to Be Counted as WHO-Analogue Fibers	
	Long individual fibers with $L \geq 5 \mu\text{m}$ and $D < 3 \mu\text{m}$ and $L/D > 3$
	Long fiber-shaped agglomerates with and $L \geq 5 \mu\text{m}$, $D < 3 \mu\text{m}$ and $L/D > 3$

Table 6. Examples of counting rules for fiber numbers in EM images.

			
Intersecting fibers are counted individually, if they are separately identifiable. Here: four fibers.	For the determination of a fiber's length attached particles (e.g., catalyst, impurities) are ignored	Splitting fibers are counted as one fiber and the length is determined on the basis of the longer part	Fibers with one end outside the SEM image frame are counted as a half fiber. Here: two WHO-fibers after the upper right fiber was found to exceed 5 μm .

2.6.3. Identification of Product Fibers

Although the fiber pathogenicity paradigm is formally independent of a fiber's bulk and surface chemistry, as long as a fiber is biodurable, composition analysis is practically required to assess material-related biodurability aspects. Additionally, toxicological relevance according to the extended fiber pathogenicity paradigm [8,30] requires material information to assess the composition- and diameter-dependent rigidity aspects of fibers. In addition, last but not least, the origin and potential source of a fiber must be clarified to distinguish background fibers of, e.g., natural origin, from fibers that were released by a work process, subsequently called product fibers. Exposure to product fibers evokes occupational responsibilities. Therefore, the identity of all countable WHO-analogue fibers must be determined to correct a fiber count for non-product fibers.

Ambient dust at assessed workplaces increases the overall occupancy of a filter sample and sometimes causes difficulties in recognizing a fiber or distinguishing a product from a background fiber. For such distinctions, identification of fibers should attempt to recognize characteristic morphological features of product fibers. For our workflow, pristine product fibers that were handled at a studied workplace were dispersed in our laboratories using the vibro-fluidizer dustiness test [33]. These reference aerosols were then sampled on filters and studied for compositional and morphological characteristics with imaging conditions identical to those applied to workplace samples. An example of a direct comparison of aerosol particles collected during dustiness testing (left) and the workplace aerosol measurement (right) is shown in Figure 1. The workplace fiber in the right image resembles the product fibers in the left image with respect to length, diameter, surface structure and imaging properties like contrast, charging and edge effect.

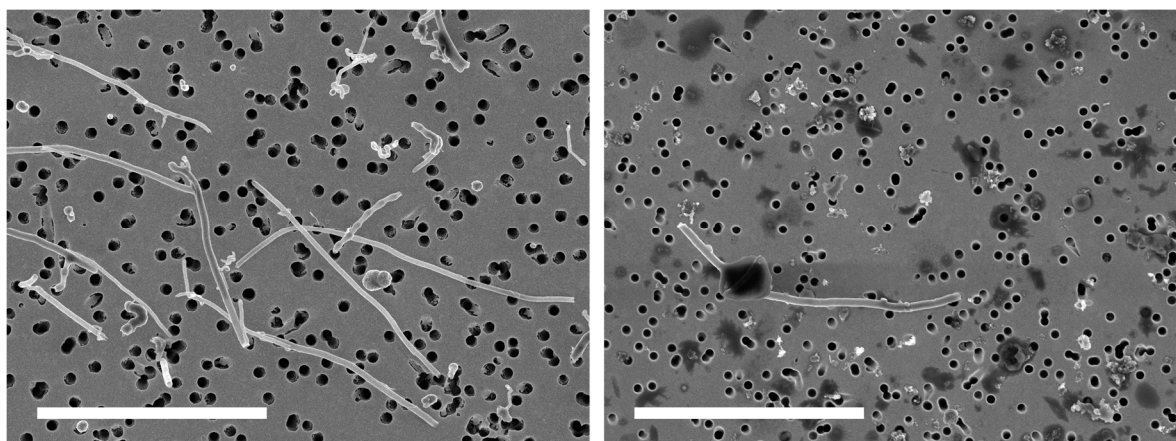


Figure 1. SEM images of the CNF material used in WP02: **(Left)** Aerosolized and sampled in the laboratory on a filter with 250 µm pore diameter. **(Right)** Filter sample of the workplace measurement with 190 µm pore diameter. The length of the scale bars is 5 µm.

Additional analyses were performed whenever fiber identification based on morphological features alone was questionable. Combining morphological and compositional information requires to spatially correlate EM images with elemental and/or chemical analyses at exactly the filter position of the fiber of interest. For nanoscale objects, the required spatial correlation accuracy can be an experimental challenge.

Information on elemental composition can be gained from energy dispersive X-ray spectroscopy (EDS). Sometimes, elemental composition alone is not sufficient, and Raman, FTIR or Laser direct infrared imaging (LDIR) spectroscopy may be required to identify chemical and structural differences. For this work, focusing on carbonaceous fibers, correlative Raman microscopic analysis was performed at a fiber's filter positions using a confocal Raman Spectrometer equipped with EMCCD detector (WITec Apyron, WITec GmbH, Ulm, Germany) with laser excitation at 532 nm and 0.5 mW power. Two example Raman analyses are presented in Figures 2 and 3. Although the analyzed nanoscale

fibers were not reliably visible in the optical microscope, the unique constellation of membrane pores in the fibers' vicinities enabled positioning the confocal Raman detection volume with an accuracy of about 50 nm. This is better than the lateral confocal resolution of about 300 nm, using a objective with 0.75 NA.

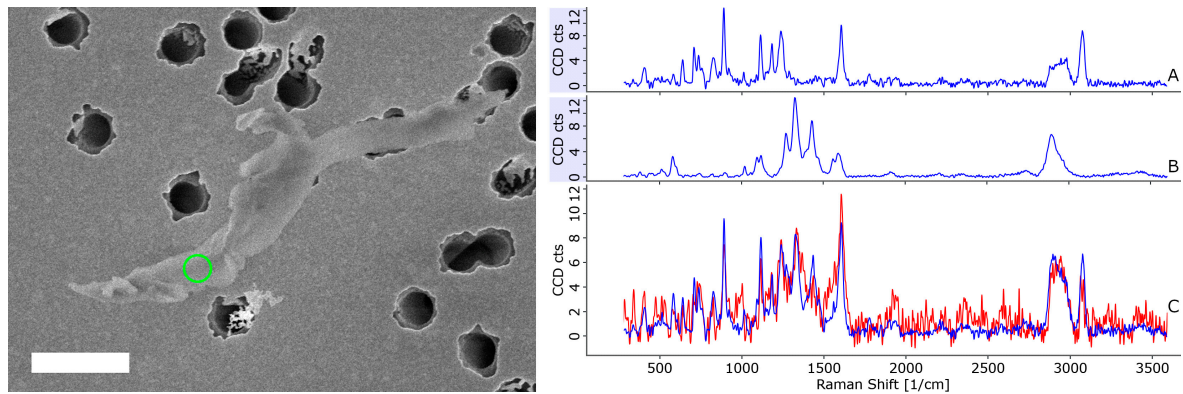


Figure 2. Raman analysis of a cellulose fiber with WHO dimensions found at WP09. **(Left)** SEM image of the fiber with the position and lateral resolution of the Raman laser spot symbolized in green. The length of the scale bar is 1 μm . **(Right)** Raman spectra of **(A)** Polycarbonate of the filter membrane as detected through the 40 μm gold coating; **(B)** Cellulose fiber of wiping paper used at the workplace; **(C)** red: Raman spectrum taken at the indicated position; blue: Superposition of spectrum **(A,B)** fitted to the red spectrum.

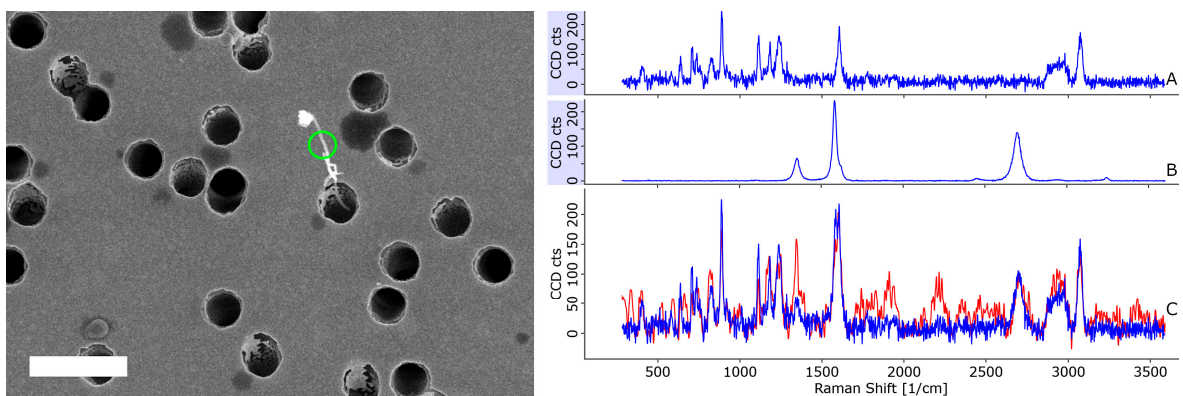


Figure 3. Raman analysis of the only MWCNT candidate fiber found at WP09. **(Left)** SEM image of the fiber with the position and lateral resolution of the Raman laser spot symbolized in green. The length of the scale bar is 1 μm . **(Right)** Raman spectra of **(A)** Polycarbonate of the filter membrane as detected through the 40 μm gold coating; **(B)** MWCNT material handled at the workplace; **(C)** red: Raman spectrum taken at the indicated position; blue: Superposition of spectrum **(A,B)** fitted to the red spectrum.

2.7. Estimating Fiber Concentrations

Analyzing a filter area A for fibers of a specific category will result in observing zero or a positive number of \hat{N} fibers. According to the counting rules in Section 2.6.1, integer and half integer values of \hat{N} are possible. The corresponding analyzed air volume $V_{\hat{N}}$ is the product of area $A_{\hat{N}}$ with the specific air volume $\varrho_V(\Phi; \tau; d_o)$, which was defined as total sampled volume V_o per total filter area A_o . An estimate \hat{n} of the true airborne fiber concentration n can be calculated from the ratio of observed fibers per analyzed air volume for known or estimated filter deposition efficiency η_{dep}

$$\hat{n} = \frac{1}{A_{\hat{N}} \cdot \varrho_V(\Phi; \tau; d_o)} \cdot \frac{\hat{N}}{\eta_{\text{dep}}} = \frac{\hat{N}}{V_{\hat{N}} \cdot \eta_{\text{dep}}} \tag{10}$$

The subsequent reasoning will deal with the observed fiber number \hat{N} , the actual measurand. Equation (10) then allows calculating airborne concentrations estimates \hat{n} from observed fiber numbers \hat{N} or true fiber number estimates N and their probability interval limits L_G, H_T, H_S .

2.7.1. Confidence versus Probability Interval Definition

Due to the high workload required for analyzing a filter area for the presence of deposited micro- and nanoscale fibers, currently only a single or very few of such measurements will be performable at a real-life workplace. Unfortunately, from a single (or very few) experiment(s), the—principally unknown—statistical distribution of the observable “number of fibers \hat{N} ” cannot be determined empirically in a Frequentist’s manner by histogramming the outcome of many repeated experiments on an atmosphere of stationary composition. As a consequence of the unknown shape of the distribution density function, no confidence interval can be specified that would make it possible to estimate a probable value range around the true fiber number N .

We therefore impose a statistical model for the distribution of our experimental results. In the case of uncorrelated deposition of airborne fibers on a filter by sampling a homogeneous aerosol and on evenly coated regions of the filter, it appears justified to assume the number of experimentally observed fibers \hat{N} to be a Poisson-distributed random variable with the probability density function $P(k; \mu) = e^{-\mu} \cdot \mu^k / k!$ with integer-valued $k \geq 0$ and real-valued expectation value μ .

The expectation value $\mu = N$ is considered to be the true value that caused the observed experimental outcome \hat{N} . Our model assumption now enables us to estimate an interval of probable values around the true number of fibers N from a single experimental observation. Mathematically correctly, such an interval is called a probability interval, not a confidence interval. Nonetheless, applied sciences generally use the term confidence interval together with an associated confidence level (CL), correctly probability level, that denotes the probability content of the probability interval between a pair of lower and an upper limit values, e.g., $[0; H_S]$ or $[L_G; H_T]$.

In the following, we will concentrate on estimating the upper limit of Poisson probability intervals of the form $[0; H_S]$, as this upper limit H_S is required for concentration limit compliance testing. Appendix C describes how lower and upper limits $[L_G; H_T]$ can be estimated to specify a probability interval around the true fiber number. Different to the traditionally used limit L_T , we recommend using the lower limit L_G since the interval $[L_G; H_T]$ exhibits the expected probability content CL, cf. Appendix D.3.

2.7.2. Upper Probability Interval Limit for Compliance Testing

A single-test upper limit H_S for a Poisson probability interval can be derived by performing a so-called left-tailed test of a single null hypothesis \mathbb{H}_0 . Our null hypothesis states that the true fiber number N to expect from sampling a specific volume V_H^S of a true airborne fiber concentration n exceeds a hypothetical fiber number H_S that would result from sampling a volume V_H^S that contains fibers with exposure limit concentration n_{EL} , see Table 7.

Table 7. Definition of the null and complement hypothesis for left-tailed testing.

Hypothesis	Left-Tail Test
Null hypothesis	$\mathbb{H}_0: N > H_S$
Complement hypothesis	$\mathbb{H}_1: N \leq H_S$

The probability of experimentally observing \hat{N} or less fibers is called the p -value and is given by the cumulated probabilities to observe $0 \dots \hat{N}$ fibers. At the so-called critical point, this p -value $p_H^S(\hat{N})$

starts to exceed a required nominal significance level α . This allows calculating the critical expectation value $H_S(\hat{N}; \alpha)$ that depends on \hat{N} and α . For a Poisson process, we find

$$\alpha \stackrel{!}{\geq} p \frac{S}{H}(\hat{N}) = \sum_{k=0}^{\hat{N}} \overbrace{\frac{H_S^k}{k!} e^{-H_S}}^{P(k; H_S)} \stackrel{\alpha = p_H^S}{\implies} H_S(\hat{N}; \alpha) = \frac{1}{2} F_{\chi^2}^{-1}(1 - \alpha; 2(\hat{N} + 1)). \tag{11}$$

More information on $F_{\chi^2}^{-1}(p; ndf)$, the p -quantile function, is given in Appendix A.3. At the critical expectation value $H_S(\hat{N}; \alpha)$, our null hypothesis \mathbb{H}_0 , which assumes the true value for the number of fibers N to exceed the critical value H_S , becomes insignificant at level α and can be rejected. The reason is that $p_H^S(\hat{N})$, the probability to observe \hat{N} or less fibers, decreases below α for any N that exceeds H_S , see Figure 4. The remaining complement hypothesis \mathbb{H}_1 is thus accepted and infers that $H_S(\hat{N}; \alpha)$ is an upper limit on the true number of fibers N . Proper selection of such an upper limit by combining Equations (10) and (11) enables us to test compliance with exposure limit concentrations.

However, the insignificance of the null hypotheses on a level of α does mathematically not infer the complement hypotheses to be significant at a level of $(1 - \alpha)$. In Appendix D.1 it is shown that the Poisson probability interval $[0; H_S]$ indeed exhibits a probability level, also called confidence level CL in applied sciences, of $CL = 1 - \alpha$. It is, therefore, justified to consider the complement hypothesis \mathbb{H}_1 probable with level CL .

For the case of zero observed fibers, Table 8 lists the minimum number of sampled fibers $H_S(0; \alpha)$ that must be expected to keep the p_H^S -value of the observation below different nominal significance levels α . Whereas Table 9 lists examples of the upper limit for zero or more observed fibers \hat{N} at fixed significance α for the single (S) and twin (T) hypothesis testing in Appendix C. Due to the Bonferroni correction, for identical upper limits a value the single test would require half the significance α of the twin test: $H_S(\hat{N}; \alpha/2) = H_T(\hat{N}; \alpha)$.

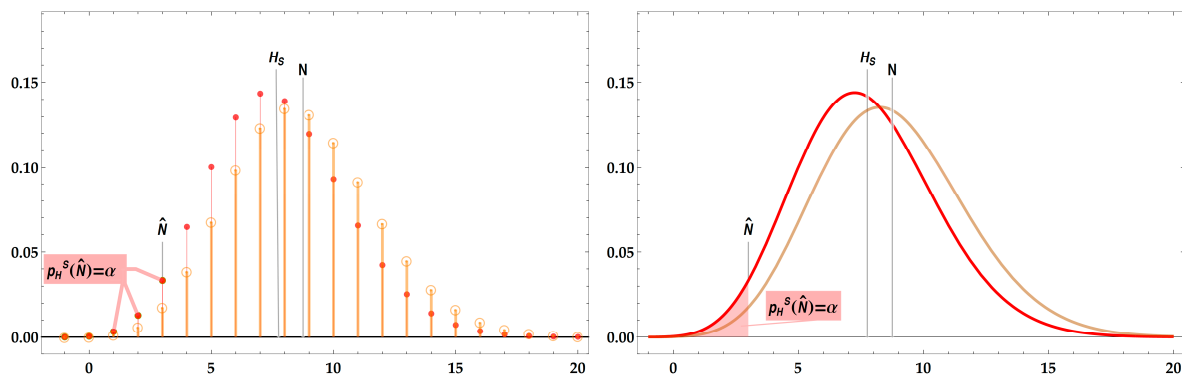


Figure 4. Illustration of the Poisson distribution model for left-tailed hypothesis testing with associated $p_H^S(\hat{N})$ -value for $\hat{N} = 0$ observed fibers at nominal significance level $\alpha = 5\%$. The left image shows the Poisson probability density, the right its continuous generalization G , cf. Equation (A9).

Table 8. Minimum number of fibers $H_S(0; \alpha)$ to expect to keep the p -value for observing zero fibers below the nominal significance level α .

Upper Compliance Limit $H_S(0; \alpha)$ at Nominal Significance Level α						
α	10 %	5 %	2.5 %	0.3 %	0.01 %	0.0001 %
$H_S(0; \alpha)$	2.303	2.996	3.689	5.809	9.210	13.815

Table 9. Upper limits of the probability intervals $H^S(\hat{N})$ and $H^T(\hat{N}; \alpha) = H^S(\hat{N}; \alpha/2)$ as derived from the single (Section 2.7.2) and the two-hypotheses (Appendix B) tests for \hat{N} observed fibers and a per-tail significance levels of $\alpha = 5\%$ and $\alpha/2 = 2.5\%$, respectively. The single-test upper limit H_S is by a fraction of $\delta(\Delta H) = (H_T - H_S)/H_S$ smaller than the upper limit H_T from twin testing.

Upper Probability Interval Limits for \hat{N} Observed Fibers and a Significance Level $\alpha=5\%$											
\hat{N}	0	1	2	3	5	10	15	30	50	100	150
$H_S(\hat{N}; \alpha)$	2.996	4.7	6.3	7.8	10.5	17.0	24.7	40.7	63.3	118	176
$\delta(\Delta H)$	–	17%	15%	13%	11%	8%	7%	5%	4%	3%	2%
$H_T(\hat{N}; \alpha)$	–	5.6	7.2	8.8	11.7	18.4	23.1	42.8	65.9	122	171

2.7.3. Limit Compliance Testing for Reducing the Workload

The single-test upper limit H_S from Section 2.7.2 is central for reducing the workload of the proposed measurement strategy even further than is possible by imposing a cut-off diameter alone. For our intention of exposure limit control, we should initially not aim at estimating an absolute fiber concentration and its associated probability interval. The reason is that this concentration assessment requires analyzing filter areas which, at the exposure limit concentration n_L , let expect about 15 or more fibers. This number of observed fibers would allow obtaining a probability interval of about 100% relative size and below, cf. Table A2 in Appendix D.4. Instead, we should test whether the workplace concentration n does not exceed our limit-of-detection, as defined in Appendix A.1, which was adjusted to be just equivalent to the exposure limit n_{EL} . In this way, already for the case of observing zero fibers, exposure limit compliance can be tested, provided the probability of observing more than zero fibers is insignificant at a level of α .

For a Poisson process, this is the case if the fiber expectation value equals $H_S(\hat{N} = 0; \alpha)$, as discussed subsequently. Several such $H_S(\hat{N} = 0; \alpha)$ fibers are expected on a filter area A_H^S that has sampled an air volume V_H^S containing exactly $H_S(\hat{N} = 0; \alpha)$ fibers at the (hypothetically true) exposure limit concentration n_{EL} . This compliance testing approach can also be generalized to cases in which actually more than zero fibers are observed. The fiber expectation value of the Poisson process must then be increased to $H_S(\hat{N}; \alpha)$ to render the probability of observing more than \hat{N} fibers insignificant at a level of α . Consequently, the filter area A_H^S to analyze must have sampled the air volume $V_H^S = H_S(\hat{N}; \alpha)/n_L$, with a deposition efficiency η_{dep} at the exposure limit concentration n_{EL} to be tested

$$A_H^S = \frac{1}{n_{EL} \cdot \eta_{dep} \cdot Q_V(\phi; \tau; d_o)} \cdot H_S(\hat{N}; \alpha). \tag{12}$$

Such an approach, using solely an estimate of the upper probability interval limit, is justified and sufficient, since the lower limit on the concentration estimate is obsolete when testing whether a concentration surmounts a specific exposure limit. However, it must be noted that the single-test upper limit $H_S(\hat{N}; \alpha)$ is actually lower than the twin-test upper limit, $H_S(\hat{N}; \alpha) < H_T(\hat{N}; \alpha)$, which was derived from a two-hypotheses test in Appendix A, due to the different significance levels α and $\alpha/2$, resulting from the Bonferroni correction, cf. Appendix C. For exposure level compliance testing, it is, therefore, not correct to take $H_T(\hat{N}; \alpha)$ as the upper limit, since it corresponds to a significance of $\alpha/2$ for single hypothesis testing.

The algorithm to follow for our limit value compliance test strategy is schematized in Section 2.9.

2.8. Online versus Offline Analysis

Traditionally, filter samples are inspected in electron microscopes by a workflow that will be called *online* in the following. A selected area of a filter is first imaged and then directly analyzed by the operator who recognizes fiber morphologies, and traces their full length and performs composition analysis by EDS before moving to the next filter area. That person must therefore be experienced in

EM microscopy, EDS analysis and fiber categorization. The online approach is efficient if the fiber categorization expertise is frequently required directly at the microscope.

However, as Table 4 shows, the number of images to acquire and analyze to identify presumably very few submicroscale fibers can become very large. Therefore, offline image inspection may be a more efficient approach if many images must be acquired before a fiber is finally encountered and requires categorization expertise. While the online approach saves images only for documentation purposes, the offline approach is solely based on stored images that are searched for fibers only after completion of a filter mapping run.

Table 10 illustrates different strategies for delegating different analysis steps to personnel of differing expertise and for distributing the workload to a team. It is a benefit of offline analysis that the microscope does not need to be operated by a fiber expert, but filter imaging can be performed by standard EM operators, or can even be automatized. Automated imaging can make the best use of (generally limited) microscope operation hours, e.g., by overnight acquisition, and can guarantee image acquisition at algorithmically or truly randomly chosen filter positions.

Table 10. Possible workflows for online, semi-automated and offline inspection of substrates containing fibers by morphological and chemical analysis using electron microscopy (EM).

Analytical Step		Offline		Offline with Automation		Online
EM image acquisition	1st	EM expert	}1st	Computer	}1st	Combined EM and fiber expert
Recognition of fibers	2nd	Trained users				
Analysis of composition	3rd	EM expert	2nd			
Categorization of fibers	4th	Fiber expert	4th			

Likewise, the task of recognizing and localizing rare fibers in a huge amount of image pixel data can be performed by non-experts or even software. Only after localization of “something resembling a fiber” on a filter is its imaged morphology reviewed by a fiber expert who decides whether additional imaging or material analysis is required prior to final categorization and counting. This may be necessary if the fiber material needs to be identified and/or if a fiber’s length cannot be categorized since it is not fully contained in the image. This probability of a fiber to not be contained can be reduced by acquiring images extending over several tens of micrometers. For some fiber materials, chemical identification may not be necessary or possible, e.g., due to a very characteristic morphology, EDS-insensitive composition or a fiber volume insufficient for EDS analysis. Re-measurement may therefore become a rare necessity, which would increase the efficiency of the offline analysis workflow.

If additional EM-, EDS- or, e.g., Raman-based analyses of fiber candidates should be necessary, the filter sample must be re-loaded into the microscope and be re-aligned to the orientation that was used during the initial imaging run. In our experience, a high-accuracy EM stage together with three or more needlepoint marks in the outer rim of a filter can achieve an alignment reproducibility of a few micrometers [34]. This is generally sufficient to re-address and recognize those previously stored, in order to be able to detect fibers with image frames several tens of micrometers in size.

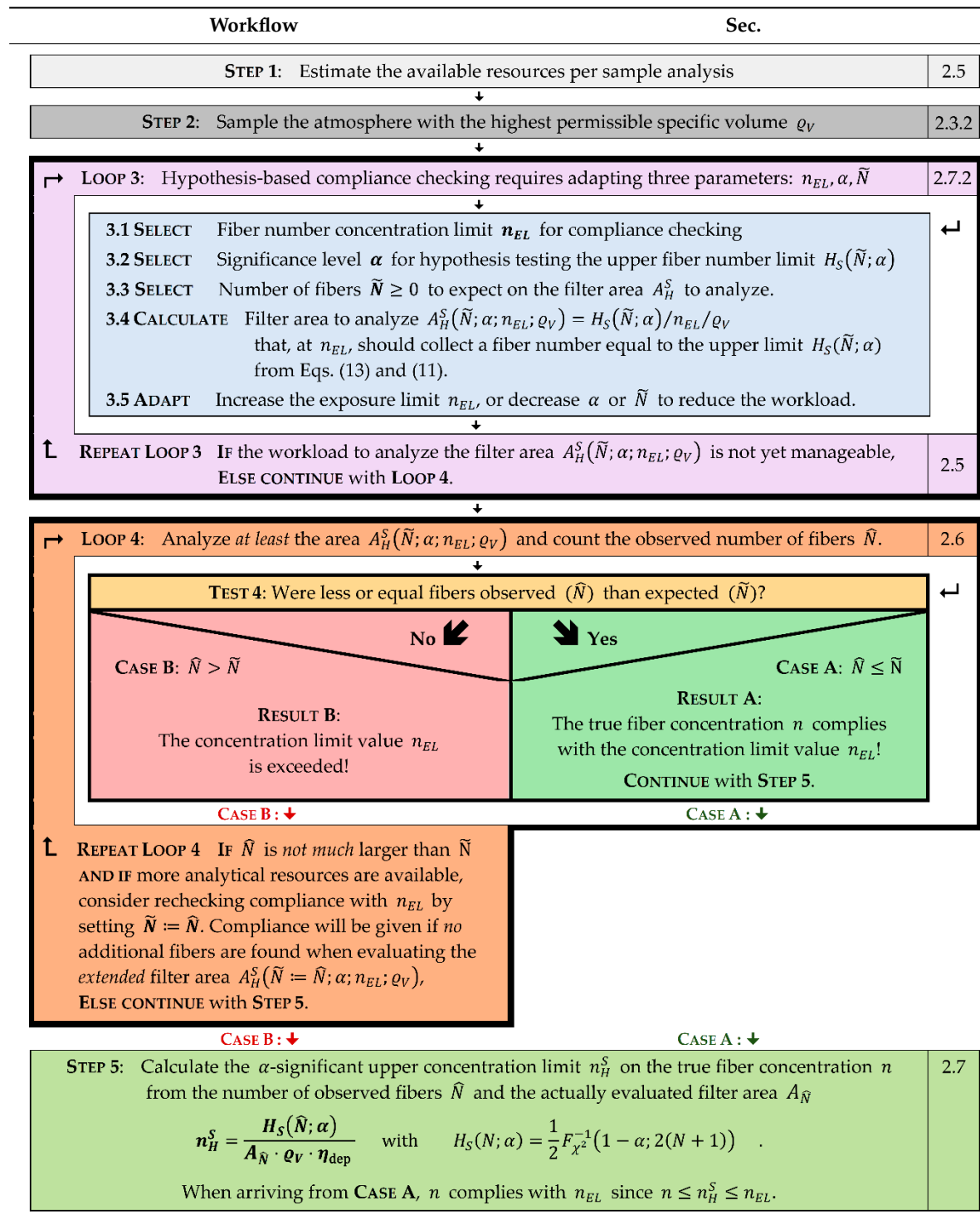
To be able to visually recognize fibers with diameters down to the fiber cut-off value on a computer monitor, not only the pixel resolution during EM imaging must be chosen appropriately but also the display conditions. It is essential to perform the fiber search at pixel-accurate scaling, so that one image pixel corresponds to at least one monitor screen pixel. This requirement, however, restricts the online image size to the EM’s monitor screen size, currently to about 1600 × 1200 pixels. Images acquired for offline analysis can, which is a benefit, be significantly larger. However, such multi-megapixel images must be inspected at pixel-accurate zoom levels or higher to exploit the full information content and to be able to detect fibers just one or two pixels in diameter. Dedicated image visualization and annotation software can help to streamline the pixelwise inspection of filter areas, document the overall progress and store discovered fiber locations and snapshots of interesting objects. The object

recognition reliability of algorithm- or machine learning-based image analysis techniques critically depends on the separability of fiber morphologies and filter surface structures. Especially recognition of complex, tangled fiber morphology is subject of on-going research [35,36].

2.9. Detailed Analysis Workflow

In Section 2.1, the general analysis workflow was introduced. Here, in Table 11, the filter evaluation part and result calculation is further detailed.

Table 11. Data evaluation workflow schematized as Nassi-Shneiderman-like diagram.



Single null hypothesis testing according to Section 2.7.2 requires evaluation of a filter area A_H^S that expects to find \tilde{N} fibers at the tested limit concentration n_{EL} . If the number \hat{N} of observed fibers is less than or equal to the expected number \tilde{N} , the true fiber concentration n is in compliance with the limit at the probability (confidence) level CL . The limit concentration n_{EL} and confidence level CL may be fixed by an implemented regulation or measurement guideline. The workload can then only be minimized by selecting the expected number \tilde{N} as zero.

Otherwise, the estimated upper limit n_H^S on the true fiber concentration n exceeds the compliance limit n_{EL} . However, if only a few more fibers are observed (CASE B of Table 11) than were expected, e.g., $\hat{N} = \tilde{N} + 1$, additional work may be invested in LOOP 4 of Table 11 for re-checking compliance with n_{EL} by expecting no additional fibers to be found during evaluation of an extended filter area, which expects to find \hat{N} fibers at concentration n_{EL} . If really no additional fibers are found on the extended filter area, compliance with n_{EL} can be stated based on a larger evaluated air volume.

3. Experiments

The measurement strategy proposed here was tested in a series of 14 workplace measurements to test its practical applicability and evaluate its relevance for exposure assessment.

3.1. Filter Deposition Efficiency

MWCNT test aerosols were generated using the vibro-fluidization technique [33] to compare the fiber deposition efficiency of filters with different track-etched pore diameters and porosities ranging from 250–750 nm and 10–20%, respectively. The data compiled in Table 12 and Figure 5 do not reveal obvious differences in fiber deposition efficiencies, especially not for WHO-analogue fibers longer than 5 μm. For the subsequent evaluation of fiber counting data on filters with 200–400 nm pore diameter and 10 % porosity, a WHO-fiber deposition efficiency of $\eta_{dep} = 1$ was assumed.

Table 12. Comparison of track-etched filters with different pore diameters and porosities. A test aerosol was generated by means of vibro-fluidization [33] and collected on the different filters. A total area of 0.054 mm² of each filter of 25 mm diameter was evaluated at random filter positions.

Property	Filter 1	Filter 2	Filter 3	Filter 4
Pore diameter	250 nm	300 nm	550 nm	750 nm
Porosity	9%	17%	20%	16%
Number of particles	3542	4383	2290	3179
Fibrous ¹	53%	47%	51%	59%
Non-fibrous ²	47%	53%	49%	41%
Mean fiber length	879 nm	931 nm	879 nm	944 nm

¹ Fibers with aspect ratio greater than 3. ² Spherical particles with aspect ratio less than 3.

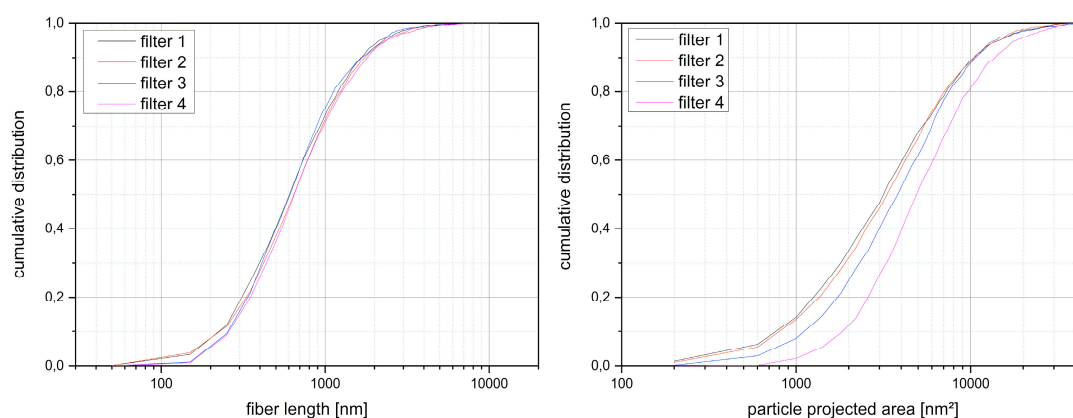


Figure 5. Cumulative length and projected area distribution of fibrous and non-fibrous particles.

3.2. Investigated Workplaces

Exposure assessments using the proposed measurement strategy were conducted at workplaces (WPs) that handled nanoscale fibers or nanofiber-containing materials. Various activities were monitored that were performed mainly in research institutes within the framework of research projects on a laboratory or pilot scale. In total, the following 14 different work processes were studied as specified in Table 13.

Table 13. The proposed measurement strategy was studied at the following 14 workplaces.

No.	Monitored Worktask
WP01	Dispersing and drying of MWCNT powders inside a glovebox
WP02	Sawing of bars consisting of a MWCNT/CNF-metal-composite [37]
WP03	Facing of MWCNT/CNF-metal-composites on a lathe
WP04	Vibro-fluidizer dustiness testing of MWCNT powders inside a workbench
WP05	CVD production of MWCNTs
WP06	CVD production of SWCNTs
WP07	Dispersing of MWCNT powders into a polymer matrix using a three-roll mill
WP08	Spreading of a MWCNT-containing suspension on a substrate
WP09	Venturi dustiness testing of MWCNT powders inside a test chamber
WP10	Extrusion of a MWCNT containing dispersion
WP11	Weighing and mixing of MWCNT/SWCNT powders and MWCNT-containing dispersions
WP12	Evaporation of a gold nanorod-containing suspension
WP13	Sawing of a CFRP sheets containing MWCNTs
WP14	Tensile testing of CFRP sheets containing MWCNTs

At each workplace, filter sampling was conducted at several sites: (1) Personal measurements for individual exposure assessment in the breathing zone (BZ); (2) stationary measurements in the nearfield (NF) close to the emission source; and (3) stationary measurements in the farfield (FF) at a distance of approximately 4–5 m from the emission source. (4) Background measurements were performed beforehand to determine the occurrence of ubiquitous dust particles and simultaneously to the work tasks at an outdoor location to monitor environmental sources.

3.3. Measurement Devices

Condensation particle counters (CPC, model 5.430, Grimm Aerosol GmbH, Ainring, Germany, measuring range 5 nm to ca. 3 μm) were used for monitoring the ultrafine particle dust load in the background and in the nearfield of the studied process [38,39]. These online measurement devices provide times series of number concentrations but provide no information on the morphology or origin of the detected particles. CPCs rely on light scattering and results are known to be unreliable for black and high aspect-ratio particles. Despite these limitations, CPC concentrations can warn of high ambient dust levels that may make it necessary to reduce the sampling flow rate.

Open-face filter sampling heads with cowl were used that are admitted for workplace aerosol sampling in accordance with the conditions described in German VDI 3492 (VDI 3492 sampling head, aluminum, GSA Messgeräte GmbH, Ratingen, Germany). These filter heads were equipped with gold-coated track-etched polycarbonate membrane filters with a diameter of 25 mm and a pore diameter of 400 nm (APC GmbH, Eschborn, Germany). When clamped into the filter, the effective (open) diameter was $A_o = 22$ mm. The configuration allows achieving high deposition efficiencies η_{dep} for nanoscale fibers together with the required high airflow using standard air sampling pumps. For the subsequent calculations, a deposition efficiency of $\eta_{\text{dep}} = 1$ was assumed, cf. Section 2.3.1.

3.4. Sampling Parameters

Sampling duration and flow rate were determined based on process parameters. The sampling time had to be adapted to the duration of the process under investigation. Therefore, only the flow rate

is variable within a range that is limited by the DGUV-recommended inflow velocity of 2–20 cm/s [26]. For an open filter diameter of $A_o = 22$ mm, this corresponds to a sampling flow rate ranging from 0.5 to 4.5 L/min. To keep the effort for the evaluation as low as possible, the flow rate should result in a specific volume q_V as high as possible in order to obtain high deposition density and, consequently, smaller workload during image acquisition and evaluation. High ambient dust load of the specific workplace should be taken into account as they may limit the permissible specific volume.

3.5. Image Acquisition by SEM

The collected filter samples were analyzed by SEM (Hitachi SU8030, Hitachi High-Technologies Europe GmbH, Krefeld, Germany) without further sample preparation. At randomly chosen filter positions, a previously determined image number were acquired to cover at least the filter area A_H^S . The visual evaluation of the images was performed offline by trained personnel, cf. Section 2.8. To be capable of detecting WHO-analogue fibers down to about 20 nm fiber diameter, i.e., WHO₂₀-fibers, during the image evaluation step, the following SEM image acquisition parameters were applied:

- Acceleration voltage: 3 kV
- Pixels per image: 5120×3840 , i.e., 19.2 megapixels
- Pixel size s and achieved resolutions r : 5.0 nm, 8.3 nm, or 12.4 nm.

As described in Section 2.5.1, a cut-off diameter of 20 nm was defined to reduce the analytical workload. The pixel sizes and SEM resolutions chosen here allowed to reliably visualize fibers with a diameter of 20 nm. If exclusively thicker fibers are to be counted, this pixel size could be increased.

3.6. Identification of Product Fibers

The identity of all counted fiber candidates was carefully examined by means of either morphological features alone or by supplementary Raman analysis.

4. Results

The proposed workflow was conducted and evaluated for 14 very different workplaces, cf. Table 13. For each workplace, one filter sample was taken at each of the following locations: In the nearfield of the emission source, in the farfield and in the personal breathing zone of an employee, cf. Section 3.2. At workplaces where exhaust ventilation or local enclosures shielded the emission source, additional measurements were performed inside fume hoods or glove boxes. The sampling during the actual process was complemented by two different types of background measurements, one performed before the start of activities in the working area, the other performed simultaneously at an outdoor location.

4.1. Sampling Parameters

According to the DGUV Information [26], the standard flow rate for the collection of aerosols at the investigated workplaces was 4 L/min. However, for our studies it was necessary to increase the flow rate to 6 L/min for work processes of short durations below 2 h in order to maximize the specific volume q_V , cf. Table 14. Such a high-volume flow rate as 6 L/min could only be used at very clean workplaces to avoid overloading the filter samples with generally ubiquitous microscale dust particles. At the workplaces investigated here, we generated a well evaluable filter loading with the selected sampling parameters. In case of very high concentrations of ambient dust, it may be necessary to reduce the flow rate. The ambient dust load can be estimated beforehand with a particle counter and can serve as orientation for the selection of the flow rate. If necessary, several measurements with different flow rates are appropriate. In Figure 6, the time series data of the CPC during the work tasks WP03 and WP12 are shown as an example. The work process at WP03 (composite facing) took 2.7 h. For aerosol sampling, 4 L/min were used. With a mean CPC particle number concentration of $(18,751 \pm 7702) \text{ \#/cm}^3$ a filter loading was obtained with reliably recognizable fibers. At workplace

WP12 (dispersion evaporation), a higher flow rate of 6 L/min was chosen for aerosol sampling on account of the very short process time of 1.4 h. Due to the comparatively low mean CPC particle number concentration of $(530 \pm 44) \text{ \#/cm}^3$ this higher flow was permissible.

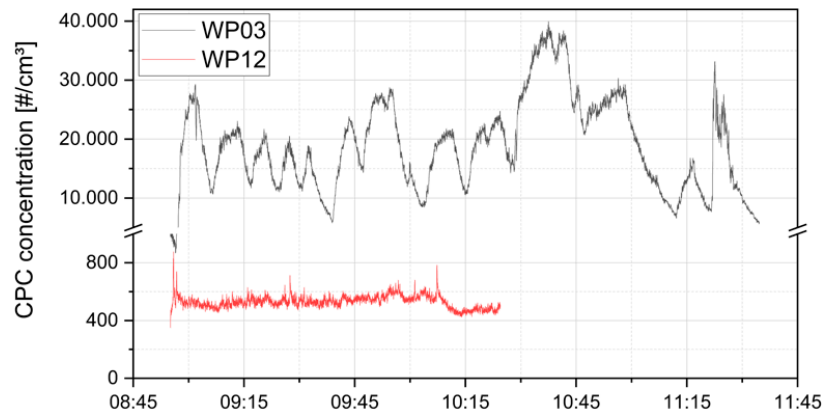


Figure 6. Particle number concentration as measured with the CPC during WP03 and WP12. For WP03 4 L/min and for WP12 6 L/min were used for filter sampling.

4.2. Calculation of Evaluation Parameters

For the process measurements in the nearfield, which had a duration of 1.4 to 7.2 h and flow rates of 4 to 6 L/min were used, the number of SEM images to be evaluated for the hypothesis test ranged between 41 and 178. For automatic SEM acquisition, about 110 s per image was required after initial position calibration of at least three reference points of the filter sample, resulting in a total image acquisition time of 1.5 to 6 h. For the subsequent software-supported visual analysis of these images, a trained human evaluator typically required about 3 min per 20 megapixels of image data, resulting in a total image evaluation time of 2 to 9 h. However, the actual time requirement will depend strongly on the filter loading and the experience of the evaluator, the filter loading and the number of fibers to be morphologically characterized. With these assumptions, the total time requirement for evaluating one filter sample typically ranges between 3.5 and 15 h.

4.3. Compliance with Benchmark Exposure Limit

For all collected filter samples of the different workplaces, the analysis was performed according to the proposed measurement procedure, as described in Table 11. In total, we found no product fibers at six workplaces. At five workplaces the analysis found no objects with WHO₂₀-fiber dimensions. Consequently, for these 11 workplaces, the true airborne WHO₂₀-fiber concentration was significantly below the German benchmark concentration of $n_{EL} = 10,000 \text{ WHO}_1/\text{m}^3$, ignoring fibers thinner than 20 nm, cf. Table 14.

At three of the investigated 14 workplaces, product fibers with WHO₂₀-fiber dimensions were observed on the evaluated filter area. Sawing of composite metal bars containing MWCNTs and CNFs at WP02 led to the observation of $\hat{N}_{WP02,NF} = 5.5 \text{ WHO}_{20}$ -objects on the nearfield aerosol sample, see Figure 7, which were morphologically identified as CNFs. This nearfield result was supported by the observation of $\hat{N}_{WP02,BZ} = 5 \text{ WHO}_{20}$ -fibers on the personal breathing zone and of $\hat{N}_{WP02,FF} = 4 \text{ WHO}_{20}$ -fibers on the farfield sample.

According to STEP 5 in Table 11, at a significance level of $\alpha = 1 - CL = 5 \%$, upper limits on the true WHO₂₀-fiber concentration can be estimated for the nearfield, the personal breathing zone and the farfield as follows

$${}_{WP02,NF} n_H^S = 37,068 \text{ WHO}_{20}/\text{m}^3, {}_{WP02,BZ} n_H^S =, {}_{WP02,FF} n_H^S = 30,554 \text{ WHO}_{20}/\text{m}^3$$

with the evaluated filter areas.

$${}^{WP02,NF}A_{5,5} = 0.066 \text{ mm}^2, {}^{WP02,BZ}A_5 = 0.074 \text{ mm}^2, {}^{WP02,FF}A_4 = 0.071 \text{ mm}^2, \text{ respectively}$$

With a probability exceeding 95 %, the corresponding fiber concentration thus does not comply with the German benchmark limit. For the $\hat{N}_{WP02,NF} = 5.5$ WHO₂₀-fibers observed, the span of the probability interval $[n_L^G; n_H^T]$ relative to the estimate \hat{n} for the true concentration n of about $(n_H^T - n_L^G)/\hat{n} = 180$ % is very large, cf. Appendix C,

$${}^{WP02,NF}\hat{n} = (18,234 \pm \frac{41,002}{8303}) \text{ WHO}_{20}/\text{m}^3.$$

An attempt to extend this measurement in order to retest compliance according to CASE B and LOOP 4 of Table 11 would have required enlarging the evaluated filter area ${}^{WP02,NF}A_{5,5}$ by a factor of $H_5(6; \alpha)/(0; \alpha) \approx 4$ and to expect no additional fibers to be found on the enlarged area. This was considered a highly unlikely endeavor and emphasizes the result that the workplace atmosphere did not comply with the tested fiber concentration limit.

Additionally, the aerosol samples of WP13 (sawing of CFRP composite sheets containing CFs and MWCNTs) and of WP14 (tensile testing of the same composite sheets) contained many particles that matched the criteria of WHO₂₀-fibers. They were apparently emitted during these processes by fracturing of CFs along their longitudinal axis [40], whereas no MWCNT-objects of the composite were found. Applying our measurement procedure, a total of $\hat{N}_{WP13,NF} = 144$ and $\hat{N}_{WP14,NF} = 78.5$ WHO₂₀-fragments of the CFs were identified on the nearfield filter samples of WP13 and WP14, respectively, cf. Table A2 and Figure 8. The upper limits of the true concentration for a significance level $\alpha = 5\%$ are ${}^{WP13,NF}n_{HS} = 956,001 \text{ WHO}_{20}/\text{m}^3$ and ${}^{WP14,NF}n_{HS} = \text{m}^3$ based on the evaluated filter areas ${}^{WP13,NF}A_{144} = {}^{WP14,NF}A_{78.5} = 0.151 \text{ mm}^2$. Therefore, the tested benchmark concentration of $10,000 \text{ WHO}_{20}/\text{m}^3$ was exceeded by at least an order of magnitude [40]. The farfield concentrations determined from $\hat{N}_{WP13,FF} = 10$ and $\hat{N}_{WP14,FF} = 0$ WHO₂₀-fragments were considerably lower ${}^{WP13,FF}n_{HS} = 56,726 \text{ WHO}_{20}/\text{m}^3$ and ${}^{WP14,FF}n_{HS} = 10,464 \text{ WHO}_{20}/\text{m}^3$ with filter areas $A_0 = 0.151 \text{ mm}^2$. This may be due to the rather short duration of these two work tasks of about 1.5 h compared to the 7.2 h of WP02, the higher mass of the CF fragments compared to MWCNTs, leading to faster dust sedimentation, and, last but not least, ventilation rate and room volume differences.

Since at WP13 and WP14 considerably more than 15 WHO₂₀-fragments were observed, it appears meaningful, cf. Table A2 in Appendix D.4 to report an estimate \hat{n} for the true concentration using the probability interval limits $[n_L^G; n_H^T]$ according to Appendix C

$${}^{WP13,NF}\hat{n} = (832,519 \pm \frac{980,137}{707,408}) \text{ WHO}_{20}/\text{m}^3 \text{ and } {}^{WP14,NF}\hat{n} = (424,558 \pm \frac{529,495}{340,675}) \text{ WHO}_{20}/\text{m}^3.$$

Table 14. Performed workplace exposure assessments with indication of the parameters used for sampling in the nearfield of the emission source (outside fume hoods or safety workbenches if used) and resulting data for the SEM analysis for a tested limit concentration of $n_{EL} = 10,000 \text{ WHO}_{20}/\text{m}^3$ and a significance of $\alpha = 5\%$. The effective filter diameter of the used sampling heads was $d_o = 22 \text{ mm}$.

ID	Work Process	Material	Mean CPC Concentration [#/ cm^3]	Flow Rate [L/min]	Duration [h]	Pixel Size [nm]	Analyzed Images à 5120×3840	Analyzed Filter Area [mm^2]	Analyzed Air Volume V_S [L]	Reached Analytical Sensitivity	Detection of Product Fibers	Number \hat{N} of WHO_{20} -Product Fibers	Single-Test Upper Limit Concentration $n_H = H_S \left(\hat{N}; \alpha \right) / V_S$
WP01	Dispersing & drying	MWCNT 1 & CNF	1393	5	6.7	5.0	116	0.057	0.30	3325 F_{20}/m^3	No	0	9961 F_{20}/m^3
WP02	Composite sawing	MWCNT 1 & CNF	17,012	4	7.2	5.0	135	0.066	0.30	3315 F_{20}/m^3	Yes	5.5 CNF	37,068 F_{20}/m^3
WP03	Composite facing	MWCNT 1 & CNF	18,751	4	2.7	8.3	129	0.175	0.30	3317 F_{20}/m^3	Yes	0	9935 F_{20}/m^3
WP04	Fluidizer dustiness	MWCNT 2	1992	4	5.7	8.3	62	0.084	0.30	3319 F_{20}/m^3	No	0	9942 F_{20}/m^3
WP05	MWCNT Production	MWCNT 3	102,686	4	7.1	8.3	62	0.084	0.38	2657 F_{20}/m^3	No	0	7958 F_{20}/m^3
WP06	SWCNT Production	SWCNT	42,768	6	1.4	8.3	178	0.241	0.32	3166 F_{20}/m^3	No	0	9485 F_{20}/m^3
WP07	Dispersing at three-roll mill	MWCNT 4	4790	4	2.2	8.3	162	0.219	0.30	3306 F_{20}/m^3	Yes	0	9905 F_{20}/m^3
WP08	Dispersion spreading	MWCNT 4	3449	5	2.2	8.3	130	0.176	0.30	3321 F_{20}/m^3	Yes	0	9950 F_{20}/m^3
WP09	Venturi dustiness	MWCNT 5	1291	6	4.3	8.3	55	0.074	0.30	3322 F_{20}/m^3	Yes	0	9952 F_{20}/m^3
WP10	Composite Extrusion	MWCNT 6	3310	5	3.6	8.3	79	0.107	0.30	3305 F_{20}/m^3	Yes	0	9900 F_{20}/m^3
WP11	Weighing & mixing	MWCNT 4 & SWCNT	8874	5	6.9	8.3	41	0.056	0.30	3307 F_{20}/m^3	No	0	9907 F_{20}/m^3
WP12	Dispersion evaporation	Gold nanorods	530	6	1.4	8.3	171	0.232	0.30	3336 F_{20}/m^3	No	0	9994 F_{20}/m^3
WP13	Composite sawing	MWCNT 7 & CF	7520	5	1.5	12.4	50	0.151	0.17	5781 F_{20}/m^3	Yes	144 CF	956,001 F_{20}/m^3
WP14	Composite tensile testing	MWCNT 7 & CF	4223	5	1.6	12.4	50	0.151	0.18	5408 F_{20}/m^3	Yes	78.5 CF	512,240 F_{20}/m^3

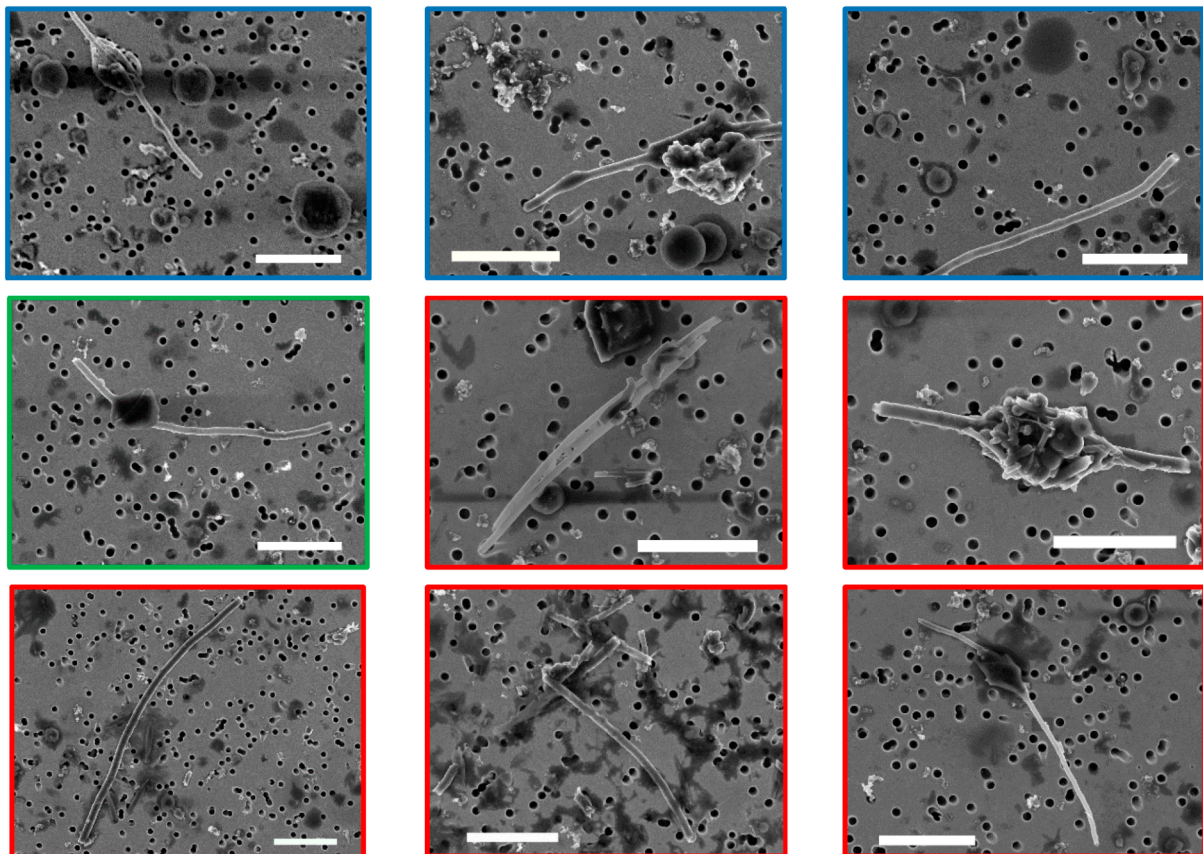


Figure 7. SEM images of all identified WHO₂₀-objects of the product CNF-material found on the nearfield aerosol sample of WP02. A green frame indicates fibers that were contained in the initial image frame. A blue frame indicates non-contained fibers recognizable as WHO₂₀-object. A red frame indicates fibers that required a re-addressing SEM measurement to be recognizable as WHO₂₀-fibers. The center image contains two WHO₂₀-fibers. A total number of $\hat{N}_{WP02,NF} = 3 \times 0.5 + 1.0 + 6 \times 0.5 = 5.5$ WHO₂₀-fibers was observed. The length of the scale bars is 2 μm .

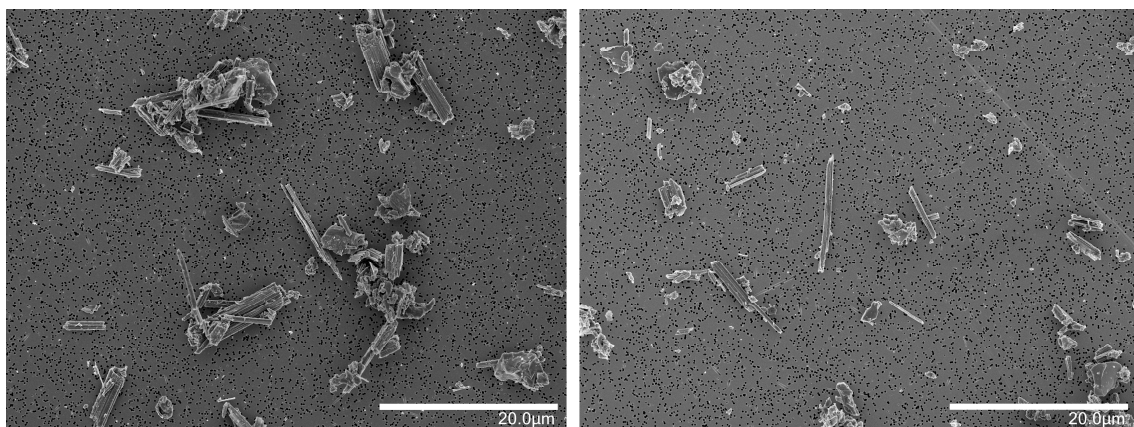


Figure 8. SEM images of nearfield aerosol samples of WP13 (left) and WP14 (right) with WHO-fragments of the processed carbon fiber. The length of the scale bar is .

5. Discussion

The proposed strategy for compliance checking concentrations of airborne nano- and microscale fibers was studied with a focus on practicability, a property that is mandatory for future implementation and routine application of new measurement concepts. At this stage, we did not aim at reporting

shift-related, statistically sound exposure assessments, which would have required repeating, sampling and evaluating work tasks three or more times [27,41]. Testing compliance of workplace atmospheres with the benchmark concentration value of 10,000 WHO₁/m³ that was published in the German TRGS 527 [13] for WHO-analogue fibers down to 1 nm diameter is still a challenge due to the impracticably high analytical effort stated above. Even with our new approach, this limit is currently only routinely testable if very thin nanofibers below 10–20 nm diameter are excluded from filter imaging and evaluation. In Section 2.5.2, toxicological and practical justifications were given for ignoring the fraction thinner than 20 nm. This enabled us to test compliance with exposure levels of 10,000 WHO₂₀/m³ here. Please note that our approach has no limitations, in principle, with respect to the included diameter range. The applied cut-off diameter can and certainly will be lowered with progress in further automating SEM image acquisition and evaluation. Currently, however, the 20 nm cut-off is crucial for rendering our testing strategy practicable and makes it the starting point for routinely monitoring compliance with fiber number-based concentration limits for airborne submicroscale fibers.

The most common significance level used in occupational health and safety is $\alpha = 5\%$, i.e., $CL = 95\%$ [23–26]. With the aim of estimating a probability interval around the true fiber number N from an observation, different to the traditionally used lower limit L_T , we recommend using the somewhat larger limit L_G , since for $\hat{N} > 0$ only the interval $[L_G; H_T]$ with $L_G(\hat{N}; \alpha) = L_T(\hat{N} + 1; \alpha)$, and not the interval $[L_T; H_T]$, exhibits the assumed probability content CL , cf. Appendix D.3. It should also be noted that when deriving both upper and lower limits $[L_G; H_T]$, the significance level α is divided by two according to the Bonferroni correction, cf. Appendix C. This is not the case for single hypothesis compliance testing with the upper limit H_S . Thus, at the same significance level α , the values of the upper limits derived from single H_S and twin hypothesis testing H_T will differ. To avoid this possible source of confusion, we recommend performing compliance testing with H_S at a significance level of $\alpha/2$ and upper and lower limit estimation $[L_G; H_T]$ at a level of α , i.e., to effectively undo the Bonferroni correction. In this way, identical values for the upper limits $H_S(\hat{N}; \alpha/2) = H_T(\hat{N}; \alpha)$ are obtained that, however, exhibit different significance levels $\alpha/2$ and α . Considering the efficiency gain of our compliance testing approach, an increased significance level of $CL = 97.5\%$ appears acceptable. The required increase of the filter area to evaluate for zero expected fibers is given in Table 8.

Our measurement strategy was successfully conducted at 14 workplaces by sampling and evaluating a total of 93 air samples. Table 14 compiles information on the workplaces and sampling parameters and reports fiber counting results for the nearfield filter samples and the corresponding upper limit concentration estimates. Since microscale fibers were already included in the image evaluation rules, the analysis of the workplace samples WP13 and WP14 performed with our nanofiber-sensitive strategy revealed that a purely microscale fiber fraction caused the observed violation of the exposure limit value for WHO₂₀-fibers [37]. For workplaces in which no WHO₂₀ product fibers were observed in the nearfield, no product fibers were found on personal or farfield samples, either. Whereas at workplaces WP02 and WP13, where the fiber concentration exceeded 10,000 WHO₂₀/m³, the personal and farfield samples also showed an excess in fibers, see Section 4.3. This supports the assumed validity of our sampling and evaluation approach.

Please note that our measurements determined process-related, not shift-related, concentrations by sampling only during specific work tasks involving the processing of fiber-containing materials, whereas established exposure limits are generally defined as shift-related (eight hours) averaged values. Thus, extrapolation to shift values may be necessary. More results of this measurement campaign have been or will be reported in dedicated workplace- and material-related publications [37,40].

The decision as to whether fibers observed on a filter were released from materials handled or machined at the workplace is crucial for deriving airborne concentrations of product fiber and for assigning occupational safety responsibilities. For the present study, both pristine product fiber and background aerosol samples were analyzed with SEM to identify characteristic morphological features that allow distinguishing release of product from background fibers. However, since morphology alone does not always allow unambiguous identification, additional information on elemental composition

should be gained from, e.g., EDS. In our case of carbon-based materials, EDS was not appropriate to distinguish carbon fibers from polymer or cellulose background fibers. Raman or FTIR spectroscopy should therefore be applied to identify chemical and structural differences of fibers located on a filter. By spatial correlation of SEM and Raman microscopic analyses, we were able to identify different CNT materials and carbon fiber fragments and to reliably distinguish them from background fibers.

Not only the identification of fibers, but also their categorization, can be difficult. An inter-laboratory comparison that applied the counting rules proposed here to highly occupied filter samples revealed differences in the categorization of (1) individual self-crossing fibers, (2) pair- or group-wise crossing fibers, or (3) loosely agglomerated fibers. Especially the classification decision for fiber-containing objects as (A) individually countable fibers or (B) non-countable fiber agglomerates performed by different human evaluators led to significant fiber counting results [42]. The workplace samples examined here showed very low occupancy rates compared to previous samples of the inter-laboratory comparison. Therefore, the subjectivity of human evaluators in the assessment of single fibers only becomes relevant if fibrous objects are observed at all. For compliance checking an exposure limit of potentially hazardous fibers at the limit-of-detection, any ambiguity in categorizing tangled or crossed fibers as countable should be resolved in favor of countability. This increases, and may even overestimate, fiber counts, which is preferable to underestimation, as it promotes protection of exposed workers.

A single compliance check of an aerosol sample for an concentration benchmark value of $10,000 \text{ WHO}_{20}/\text{m}^3$ according to the proposed method requires the analysis of 40–180 SEM images at 5120×3840 pixels with 0.8–3.5 gigapixels, typically at 8.3 nm pixel resolution, to reach or surpass the required limit-of-detection sensitivity that, as defined in Appendix A.1, is necessary for null hypothesis testing. Due to the offline analysis approach using SEM images that were generally acquired automatically overnight, the subsequent workload could be distributed to several human evaluators. The workflow currently consumes 1.5–6 h of SEM time plus 2–9 man hours of image evaluation time per filter sample. For offline analysis, archiving position-calibrated filter samples is mandatory to be able to re-address product fiber candidates in both the SEM and Raman microscope for a second in-depth material analysis or for tracking long fibers that were not fully contained in the initially taken SEM image.

6. Conclusions

Despite compelling reports on asbestos-like pathogenicity, regulatory bodies have thus far been hesitant to implement fiber number-based exposure limits for biodurable nanoscale fibers. One reason has been a lack of a practicable strategy for assessing airborne fiber number concentrations, since inclusion of nanofibers in the range of 200–1 nm causes a 40,000-fold increase in the analytical workload compared to that for WHO_{200} -fiber number concentration determination.

The goal of the present work was to lay out a proposed compliance test strategy in detail and to study its practicability. Confirming practicability is the mandatory first step in implementing and routinely applying a new measurement concept. The 14 studied workplaces and the 93 evaluated filter samples allowed us to optimize the analysis workflow with respect to imaging and evaluation conditions and to help colleagues who study MWCNT-containing materials, mostly in research institutes, to obtain a first preliminary assessment of the effectiveness of their safety measures. At this early stage, we did not aim at reporting shift-related, statistically sound exposure assessments that would have required our partners to repeat their work tasks at least three times on consecutive days.

The large number of processed samples demonstrates that the proposed measurement strategy can indeed be employed for compliance testing concentrations of airborne fibers of possible toxicological concern with a manageable workload. Analogous to established methods for WHO_{200} -fiber fractions, our strategy includes micro- and submicroscale airborne fibers only down to a so-called critical diameter in the nanoscale. The cut-off diameter of about 20 nm proposed here was motivated by toxicological data on MWCNTs and should, when adapted to other fiber materials, be adapted considering the

extended fiber pathogenicity paradigm. The extended paradigm introduced a critical fiber rigidity which is considered responsible for asbestos-like effects of respirable biodurable WHO-analogue fibers in lung tissue.

For aerosols containing nanoscale fibers, this cut-off diameter is currently the most relevant step for arriving at practically manageable workloads. Thus, ignoring nanofibers of potentially lower toxicological relevance in the diameter range of 1–20 nm allows the reduction of the workload by a factor of 400. Additional workload reduction results from not aspiring to absolutely quantify fiber concentrations but to work at the limit-of-detection right from the start. For such fiber non-appearance testing, the fiber sampling and detection process was assumed to be governed by Poisson statistics. The fiber counting result on a filter area, which was carefully adjusted to a required confidence level and a specific exposure limit value, either confirms or rejects the hypothesis of compliance to an upper limit on the true fiber concentration.

As set out in the Appendix, in the case of sparse fiber observations, as is typical for testing low concentration limits, testing compliance with an upper limit requires the analysis of filter areas considerably smaller than those required for estimating true fiber concentrations, cf. Appendix D.4. We therefore recommend starting with performing upper limit compliance testing and to only report an estimate for the true concentration \hat{n} if the observed number of fibers \hat{N} is large enough to result in a small probability interval that actually constrains the estimate in a practically valuable manner. To avoid different values for the upper limit from compliance testing n_H^S and confidence interval limits estimation $[n_L^C; n_H^T]$, we recommend performing compliance testing at a significance level of $\alpha/2$, and confidence interval limit estimation at a level of α . This effectively undoes the typically applied Bonferroni correction, cf. Appendix C, and results in identical values of differing statistical significance.

We conclude that the application of the proposed testing strategy for nano- and microscale fibers to 14 very different workplaces showed the resulting workload to be high but well manageable. Our approach thus enables the occupational health community to routinely control fiber number-based concentration limits at a level of 10,000 WHO₂₀/m³ for nano- and microscale fibers with diameters of 20 nm and above. Automated microscopes, re-addressable, position-calibrated filter samples allow performing the image evaluation in so-called offline mode. This makes it possible to distribute the task of visually searching for fibers on EM images with a total of about 10⁹ pixels per sampling to trained personnel, thus keeping the EM operator free to perform the imaging. Our workflow currently requires 1.5–6 h of SEM time plus 2–9 man hours of image evaluation time per filter sample. Progress in the degree of automation of image acquisition and object recognition is already underway and will not only further lower the costs of analysis and render the proposed strategy a standard service for workplace exposure assessment but will also allow including fibers thinner than 20 nm in an evaluation in the near future.

Author Contributions: Conceptualization, A.M.-P., D.B. and S.P.; Data curation, D.B., N.D., D.P., B.K.S., C.T. and D.W.; Formal analysis, A.M.-P. and D.B.; Funding acquisition, S.P.; Investigation, D.B., N.D., D.P., B.K.S., C.T. and D.W.; Methodology, A.M.-P., D.B. and S.P.; Project administration, D.B.; Resources, A.M.-P., D.B. and S.P.; Supervision, S.P.; Validation, A.M.-P. and D.B.; Visualization, A.M.-P. and D.B.; Writing—original draft, A.M.-P. and D.B.; Writing—review & editing, A.M.-P. and D.B. All authors have read and agreed to the published version of the manuscript.

Funding: This research was partially funded by Deutsche Gesetzliche Unfallversicherung (DGUV), grant number FP-0409.

Acknowledgments: Helpful discussions with T. Bruun, K. Kämpf, N. Kersten, M. Mattenklott, C. Möhlmann and P. Steinle as well as visual SEM image evaluation by T. Alhajali, K. Rebwar and S. Schröder are acknowledged.

Conflicts of Interest: The authors declare no conflict of interest.

Appendix A. Definitions

Appendix A.1. Limit-of-Detection

The upper probability limit $H_S(\hat{N}; \alpha)$ of Section 2.7.2 is directly related to the definition of a limit-of-detection for Poisson-distributed random processes:

The limit-of-detection is given by the compliance limit that results from observing zero fibers.

According to Poisson statistics, it states that, if you find zero fibers, you may have missed $H_S(0; \alpha)$ truly present fibers. Therefore, you cannot quantify less than $H_S(0; \alpha)$ fibers, since observation of zero fibers is still in compliance with $H_S(0; \alpha)$ truly present fibers. For example, at $\alpha = 5\%$, the fiber limit-of-detection is $H_S(\hat{N} = 0; \alpha = 5\%) = 2.996$. To calculate the corresponding airborne fiber concentration-related limit-of-detection, input $\hat{N} = H_S(0; \alpha)$ into Equation (10) and calculate the result.

Appendix A.2. Analytical Sensitivity

The analytical sensitivity is defined as the minimum number of fibers you can actually observe. This is per definition one fiber, ignoring the possibility to observe “half a fiber” practice due to specific counting rules for fibers that are not fully contained in an image frame. To calculate the corresponding airborne fiber concentration-related analytical sensitivity, input $\hat{N} = 1$ into Equation (10) and calculate the result.

Appendix A.3. p-Quantile Function

$F_{\chi^2}^{-1}(p; ndf)$ is the p -quantile function for a χ^2 distribution of ndf degrees of freedom, i.e., the inverse of the cumulative χ^2 distribution [43]. As of version “Excel 2010”, $F_{\chi^2}^{-1}(p; ndf)$ is implemented in Microsoft Excel® as CHISQ.INV($p; ndf$). Mathematically, $\frac{1}{2}F_{\chi^2}^{-1}(p; ndf)$ corresponds to the inverse of the generalized regularized incomplete gamma function <https://functions.wolfram.com/GammaBetaErf/InverseGammaRegularized3>. Evaluation is possible at <https://functions.wolfram.com/webMathematica/FunctionEvaluation.jsp?name=InverseGammaRegularized3>.

Appendix B. Sampling Error Propagation

The experimental errors on sampling duration τ , airflow rate Φ and open filter area A_o give rise to uncertainties in the analyzed volume V_H^S and specific surface volume ρ_V . They affect the error on the upper limit of fibers $H_S(\hat{N}; \alpha)$ to expect on the analyzed filter area A_H^S for a selected exposure limit concentration n_{EL} . For constant airflow rate Φ , we find the following according to Equation (12) and Section 2.3.2

$$H_S(\hat{N}; \alpha) = n_{EL} \cdot \eta_{dep} \cdot A_H^S \cdot \rho_V(\Phi; \tau; d_o) = n_{EL} \cdot \eta_{dep} \cdot \frac{A_H^S}{A_o(d_o)} \cdot V_H^S(\Phi; \tau) = n_{EL} \cdot \eta_{dep} \cdot \frac{4 A_H^S}{\pi d_o^2} \cdot \Phi \cdot \tau \quad (A1)$$

with an absolute (Δ) or relative (δ) error of

$$\Delta H_S = H_S \cdot \sqrt{\frac{\Delta \eta_{dep}^2}{\eta_{dep}^2} + 4 \frac{\Delta d_o^2}{d_o^2} + \frac{\Delta \tau^2}{\tau^2} + \frac{\Delta \Phi^2}{\Phi^2}} \quad \delta \Leftrightarrow H_S = \sqrt{\delta \eta_{dep}^2 + 4 \delta d_o^2 + \delta \tau^2 + \delta \Phi^2} \quad (A2)$$

The error sources on expected fiber number $H_S(\hat{N}; \alpha)$ at exposure limit concentration n_{EL} may decrease the actually achieved significance level α . While start and end time errors on the order of minutes may be negligible for measurement durations τ exceeding an hour, relative errors of just 10% on flow Φ , open filter diameter d_o and deposition efficiency η_{dep} can already cause a δH_S of 24%. For the case of zero observed fibers and a significance level $\alpha = 5\%$, $H_S(0; \alpha) = 2.996$ exhibits an

absolute error of $\Delta H_S = H_S(0; \alpha) \cdot \delta H_S = 0.73$. In such a case, the null hypothesis significance level α that satisfies the equation

$$\alpha \stackrel{!}{=} p_H^S(\hat{N} = 0) = \sum_{k=0}^{\hat{N}} \frac{(H_S \pm \Delta H_S)^k}{k!} e^{-(H_S \pm \Delta H_S)} = e^{-(H_S \pm \Delta H_S)} \tag{A3}$$

may actually deviate from the intended significance level $\alpha = 5\%$ and lie in the range of $\alpha \in [e^{-(H_S + \Delta H_S)}, e^{-(H_S - \Delta H_S)}] = [2.4\%; 10.4\%]$. A significance increased to $\alpha = 10.4\%$ corresponds to an effectively lower probability level $CL = 1 - \alpha = 89.6\%$.

It is, therefore, important to avoid any *overestimation* of the filter deposition efficiency η_{dep} and the aerosol flow Φ as well as an *underestimation* of the open filter area by performing filter deposition studies, applying careful flow calibration as well as mechanically reliable filter support and clamping.

Appendix C. Lower L_T and Upper H_T Limits for Two-Side-Bounded Probability Intervals

There are various ways of defining and estimating probability intervals, also called confidence intervals in the applied sciences [44]. Here, the twin-test lower L_T and upper H_T interval limits for the true number of fibers N are derived. These two limits result from performing both a left-tail \mathbb{H}_0 and a right-tail \mathbb{L}_0 null hypothesis test for the nominal significance level of α . The two single-tailed hypotheses pairs are stated in Table A1.

Table A1. Definition of the two single-tailed hypotheses to derive interval limits by left- and right-tailed tests.

	Right-Tail Test	Left-Tail Test
Null hypothesis	$\mathbb{L}_0: L_T > N$	$\mathbb{H}_0: N > H_T$
Complement hypothesis	$\mathbb{L}_1: L_T \leq N$	$\mathbb{H}_1: N \leq H_T$

The associated p -values are given in Equation (A4) by the cumulative probabilities $p_L^T(\hat{N})$ to observe \hat{N} or less fibers, and $p_H^T(\hat{N})$ to observe \hat{N} or more fibers. Using the Bonferroni correction for multiple hypothesis testing, for the twin test we require a nominal significance level of $\alpha/2$ per hypothesis.

The left of Figure A1 illustrates how p_L^T or p_H^T change when varying $L_T \rightarrow L_T - \varepsilon$ or $H_T \rightarrow H_T + \varepsilon$, respectively, which renders the null hypotheses less significant, and thus constrains the interval size. Choosing $p_L^T(\hat{N}) = p_H^T(\hat{N}) = \alpha/2$ makes it possible to reject both null hypotheses as insignificant for a total significance level of α and to calculate the associated limit values $L_T(\hat{N}; \alpha/2)$ and $H_T(\hat{N}; \alpha/2)$ from

$$\frac{\alpha}{2} \stackrel{!}{\geq} p_H^T(\hat{N}) = \sum_{k=0}^{\hat{N}} \frac{H_T^k}{k!} e^{-H_T} \text{ and } \frac{\alpha}{2} \stackrel{!}{\geq} p_L^T(\hat{N}) = \sum_{k=\hat{N}}^{\infty} \frac{L_T^k}{k!} e^{-L_T} \tag{A4}$$

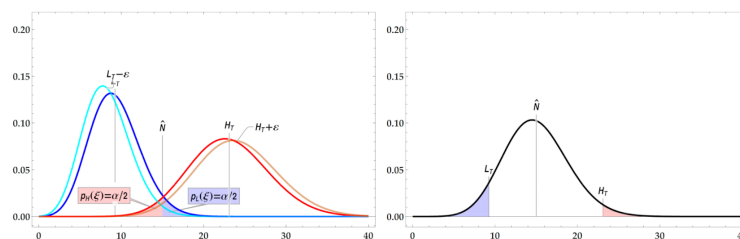


Figure A1. Illustration of the Poisson distribution models for two single-sided hypothesis tests (twin test) with associated p -values (left) and resulting probability interval (right) for the case of $\hat{N} = 15$ observed fibers, a nominal significance level $\alpha = 10\%$ and $\varepsilon = 1$.

The case of zero observed fibers, which requires single-tailed null hypothesis testing since the observation coincides with the lower limit, was dealt with in 2.7.1. For $\hat{N} > 0$, Equation (A4) offers the solutions

$$L_T(\hat{N}; \alpha) = \frac{1}{2} F_{\chi^2}^{-1}\left(\frac{\alpha}{2}; 2\hat{N}\right) \tag{A5}$$

$$H_T(\hat{N}; \alpha) = \frac{1}{2} F_{\chi^2}^{-1}\left(1 - \frac{\alpha}{2}; 2(\hat{N} + 1)\right) = H_S\left(\hat{N}; \frac{\alpha}{2}\right). \tag{A6}$$

The accepted complementary hypotheses infer the critical values to be lower and upper limits of a probability interval $[L_T; H_T]$ around the true number of fibers N . These limits correspond to those a Frequentist statistical approach [45].

However, the insignificance of the null hypotheses on a level of α does not infer the complement hypotheses to be significant at a level of $(1 - \alpha)$. As Appendix D.3 shows, to satisfy this condition requires defining a modified lower limit L_G . The correct interval around the true number that exhibits a probability content of $(1 - \alpha)$ therefore is $[L_G; H_T]$.

Appendix D. Probability Content of Poisson Intervals

Appendix D.1. Probability Content of Single-Bounded Poisson Intervals

To determine the exact probability content, called confidence level CL in applied sciences, of the Poisson probability interval $[0, H_S]$, we assume a Gamma distribution with shape $(\eta + 1)$ and scale 1 [46]. The form of its probability density function $G(\mu; \xi) := e^{-\mu} \cdot \mu^\xi / \xi!$ for real-valued ξ has a shape identical to the Poisson density function $P(k; \mu) := e^{-\mu} \cdot \mu^k / k!$ for integer-valued k . Please note the permuted arguments of these two probability density functions. For $H_S \geq 0$, this allows the use of an identity derived from the Bayesian theorem for conditional probabilities [47]

$$\underbrace{\sum_{k=0}^{\hat{N}} \frac{H_S^k}{k!} e^{-H_S}}_{p_H^S(N)=\alpha} + \underbrace{\int_0^{H_S} \frac{N^{\hat{N}}}{\hat{N}!} e^{-N} dN}_{G(N; \hat{N})} = 1. \tag{A7}$$

$CL(L_G \leq N \leq H_T | \hat{N})$

The integral of the Gamma probability density function $G(N; \hat{N})$ over the interval $[0; H_S]$ corresponds to the probability $CL(0 \leq N \leq H_S | \hat{N})$ of the true fiber number N to lie in that interval if \hat{N} fibers are observed. Since the limit H_S was derived at the critical point $p_H^S(\hat{N}) = \alpha$, the probability level is indeed

$$CL(0 \leq N \leq H_S | \hat{N}) = 1 - \alpha. \tag{A8}$$

Appendix D.2. Probability Content of Two-Side-Bounded Poisson Intervals and Improved Lower Limit

The probability content for two-side-bounded Poisson intervals can also be derived from the Bayesian theorem for conditional probabilities [47]

$$\underbrace{\sum_{k=0}^{\hat{N}} \frac{H_T^k}{k!} e^{-H_T}}_{p_H^T(\hat{N})=\frac{\alpha}{2}} + \underbrace{\int_{L_T}^{H_T} \frac{N^{\hat{N}}}{\hat{N}!} e^{-N} dN}_{G(N; \hat{N})} + \underbrace{\sum_{k=\hat{N}}^{\infty} \frac{L_T^k}{k!} e^{-L_T}}_{p_L^T(\hat{N})=\frac{\alpha}{2}} - \underbrace{\frac{L_T^{\hat{N}}}{\hat{N}!} e^{-L_T}}_{P(\hat{N}; L_T)} = 1 \tag{A9}$$

$CL(L_T \leq N \leq H_T | \hat{N})$

The integral of the Gamma probability density function $G(N; \hat{N})$ over the interval $[L_T; H_T]$ now corresponds to the probability $CL(L_T \leq N \leq H_T | \hat{N})$ of the true fiber number N to lie in that interval if \hat{N} fibers are observed [47]. Since the limits L_T and H_T were derived for $p_L^T(\hat{N}) = p_H^T(\hat{N}) = \alpha/2$, Equation (A9) can be written as

$$1 - \alpha < CL(L_T \leq N \leq H_T | \hat{N}) = 1 - \alpha + \overbrace{\frac{L_T^{\hat{N}}}{\hat{N}!} e^{-L_T}}^{P(N; L_T)}. \tag{A10}$$

The probability of the Frequentist’s interval $[L_T; H_T]$ is thus greater than CL by a value of $P(\hat{N}; L_T)$.

Appendix D.3. Defining a Corrected Lower Limit L_G

The fact that the probability level CL of the Frequentist’s interval $[L_T; H_T]$ exceeds $(1 - \alpha)$ by $P(\hat{N}; L_T)$ motivates defining an alternative lower limit L_G that is slightly larger via L_T via the Bayesian theorem

$$\underbrace{\sum_{k=0}^{\hat{N}} \frac{H_T^k}{k!} e^{-H_T}}_{p_H^T(\hat{N})=\frac{\alpha}{2}} + \underbrace{\int_{L_G}^{H_T} \frac{N^{\hat{N}}}{\hat{N}!} e^{-N} dN}_{CL(L_G \leq N \leq H_T | \hat{N})} + \underbrace{\sum_{k=\hat{N}+1}^{\infty} \frac{L_G^k}{k!} e^{-L_G}}_{=p_L^G(\hat{N})=\frac{\alpha}{2}} = 1 \tag{A11}$$

$$\frac{\alpha}{2} \stackrel{!}{\geq} p_L^G(\hat{N}) = \sum_{k=\hat{N}+1}^{\infty} \frac{L_G^k}{k!} e^{-L_G} \xrightarrow{p_L^G(\hat{N})=\frac{\alpha}{2}} L_G(\hat{N}; \alpha) = \frac{1}{2} F_{\chi^2}^{-1}\left(\frac{\alpha}{2}; 2(\hat{N} + 1)\right) \tag{A12}$$

According to Equation (A11), the probability content $CL(L_G \leq N \leq H_T | \hat{N}) = \int_{L_G}^{H_T} e^{-N} \cdot N^{\hat{N}} / \hat{N}! dN$ is exactly equal to $(1 - \alpha)$ only if it is limited by the lower $L_G(\hat{N}; \alpha) = L_T(\hat{N} + 1; \alpha)$ and upper limit $H_T(\hat{N}; \alpha) = H_S(\hat{N}; \alpha/2)$.

Appendix D.4. Sample Values and Relative Size of Different Probability Interval Limits

Table A2 shows how for small observed fiber numbers \hat{N} below about 15 fibers, the relative size of the probability interval $\delta H_T + \delta L_G = (H_T(\hat{N}; \alpha) / \hat{N} - 1) + (L_G(\hat{N}; \alpha) / \hat{N} - 1)$ with respect to the observation \hat{N} exceeds 100 %. The probability interval $[L_G; H_T]$ then does not constrain the true fiber number estimate in a practically valuable manner, instead apply compliance testing of Section 2.7.1

Table A2. Upper and lower limits of twin hypothesis testing for Frequentist (L_T and H_T) and Bayesian theorem (L_G) probability intervals as calculated from Equations (A5), (A6) and (A12) for \hat{N} observed fibers and a significance level of $\mu = 5\%$. Gray areas indicate fiber counts with relatively large intervals

Probability Interval Limits and Relative Errors for N Observed Fibers and $\mu = 5\%$ Significance										
δH_T	460%	260%	190%	130%	84%	65%	43%	32%	22%	17%
H_T	5.6	7.2	8.8	11.7	18.4	24.7	42.8	65.9	122	176
\hat{N}	1	2	3	5	10	15	30	50	100	150
L_T	0	0.2	0.6	1.6	4.8	8.4	20.2	37.4	81.4	127.0
δL_T	97%	88%	79%	68%	52%	44%	33%	26%	19%	15%
L_G	0.2	0.6	1.1	2.2	5.5	9.1	21.1	38.0	82.3	127.9
δL_G	76%	69%	64%	56%	45%	39%	30%	24%	18%	15%

References

1. Pott, F.; Friedrichs, K.H. Tumoren der Ratte nach i.p.-Injektion faserförmiger Stäube. *Naturwissenschaften* **1972**, *59*, 318. [[CrossRef](#)] [[PubMed](#)]
2. Stanton, M.F.; Wrench, C. Mechanisms of mesothelioma induction with asbestos and fibrous glass. *J. Natl. Cancer Inst.* **1972**, *48*, 797–821. [[CrossRef](#)] [[PubMed](#)]
3. Furuya, S.; Chimed-Ochir, O.; Takahashi, K.; David, A.; Takala, J. Global Asbestos Disaster. *Int. J. Environ. Res. Public Health* **2018**, *15*, 1000. [[CrossRef](#)]
4. World Health Organization. *Determination of Airborne Fibre Number Concentrations: A Recommended Method, by Phase-Contrast Optical Microscopy (Membrane Filter Method)*; World Health Organization: Geneva, Switzerland, 1997.
5. Poland, C.; Duffin, R.; Kinloch, I.; Maynard, A.; Wallace, W.; Seaton, A.; Stone, V.; Brown, S.; MacNee, W.; Donaldson, K. Carbon nanotubes introduced into the abdominal cavity of mice show asbestos-like pathogenicity. *Nat. Nanotechnol.* **2008**, *3*, 423–428. [[CrossRef](#)]
6. Kane, A.B.; Hurt, R.H.; Gao, H. The asbestos-carbon nanotube analogy: An update. *Toxicol. Appl. Pharmacol.* **2018**, *361*, 68–80. [[CrossRef](#)] [[PubMed](#)]
7. Rittinghausen, S.; Hackbarth, A.; Creutzenberg, O.; Ernst, H.; Heinrich, E.; Leonhardt, A.; Schaudien, D. The carcinogenic effect of various multi-walled carbon nanotubes (MWCNTs) after intraperitoneal injection in rats. *Part. Fibre Toxicol.* **2014**, *11*, 59. [[CrossRef](#)] [[PubMed](#)]
8. Broßell, D.; Meyer-Plath, A.; Kämpf, K.; Plitzko, S.; Wohlleben, W.; Stahlmecke, B.; Wiemann, M.; Haase, A.A.; Kämpf, K.; Plitzko, S.; et al. A Human risk banding scheme for high aspect-ratio materials. In *Synthetic Nano- and Microfibers*; Wagterveld, R.M., Wiemann, M., Eds.; WETSUS: Leeuwarden, The Netherlands, 2020; pp. 55–80.
9. ISO/TS 80004-2. *Nanotechnologies—Vocabulary—Part 2: Nano-Objects*; ISO: Geneva, Switzerland, 2015.
10. The European Commission. Commission recommendation of 18 October 2011 on the definition of nanomaterial text with EEA relevance. *Off. J. Eur. Union* **2011**, *L275*, 38–40.
11. Dodson, R.F.; Atkinson, M.A.; Levin, J.L. Asbestos fiber length as related to potential pathogenicity: A critical review. *Am. J. Ind. Med.* **2003**, *44*, 291–297. [[CrossRef](#)]
12. Health Council of the Netherlands. *Asbestos: Risks of Environmental and Occupational Exposure*; Health Council of the Netherlands: The Hague, The Netherlands, 2010.
13. German Committee on Hazardous Substances (AGS). *TRGS 527: Activities with Nanomaterials*; Gemeinsames Ministerialblatt: Hürth, Germany, 2020; pp. 102–118.
14. Stanton, M.F.; Layard, M.; Tegeris, A.; Miller, E.; May, M.; Kent, E. Carcinogenicity of Fibrous Glass: Pleural Response in the Rat in Relation to Fiber Dimension. *J. Natl. Cancer Inst.* **1977**, *58*, 587–603. [[CrossRef](#)]
15. Boulanger, G.; Andujar, P.; Pairon, J.-C.; Billon-Galland, M.-A.; Dion, C.; Dumortier, P.; Brochard, P.; Sobaszek, A.; Bartsch, P.; Paris, C.; et al. Quantification of short and long asbestos fibers to assess asbestos exposure: A review of fiber size toxicity. *Environ. Health* **2014**, *13*, 59. [[CrossRef](#)]
16. French Agency for Environmental and Occupational Health Safety (AFSSET). *Opinion of AFSSET Relating to the Proposed Occupational Exposure Limits of Chemicals in the Workplace: Asbestos Fibres: Assessment of the Health Effects and Methods used to Measure Exposure Levels in the Workplace*; French Agency for Environmental and Occupational Health Safety: Maisons-Alfort, France, 2009.
17. Stockmann-Juvala, H.; Taxell, P.; Santonen, T. *Formulating Occupational Exposure Limits Values (OELs) (Inhalation & Dermal)*; Finnish Institute of Occupational Health (FIOH): Helsinki, Finland, 2014.
18. Mihalache, R.; Verbeek, J.H.; Graczyk, H.; Murashov, V.; Van Broekhuizen, P. Occupational exposure limits for manufactured nanomaterials, a systematic review. *Nanotoxicology* **2017**, *11*, 7–19. [[CrossRef](#)] [[PubMed](#)]
19. World Health Organization. *WHO Guidelines on Protecting Workers from Potential Risks of Manufactured Nanomaterials*; World Health Organization: Geneva, Switzerland, 2017.
20. British Standards Institution (BSI). *Nanotechnologies—Part 2: Guide to Safe Handling and Disposal of Manufactured Nanomaterials*; PD6699-2:2007; British Standards Institution (BSI): London, UK, 2007.
21. National Institute for Occupational Safety and Health (NIOSH). *Current Intelligence Bulletin 65: Occupational Exposure to Carbon Nanotubes and Nanofibers*; National Institute for Occupational Safety and Health (NIOSH): Washington, DC, USA, 2013.

22. National Institute for Occupational Safety and Health (NIOSH). Analysis of carbon nanotubes and nanofibers on mixed cellulose ester filters by transmission electron microscopy. In *NIOSH Manual of Analytical Methods*, 5th ed.; National Institute for Occupational Safety and Health (NIOSH): Washington, DC, USA, 2016.
23. National Institute for Occupational Safety and Health (NIOSH). Method 7400: Asbestos and other fibers by PCM. In *NIOSH Manual of Analytical Methods*, 5th ed.; National Institute for Occupational Safety and Health (NIOSH): Washington, DC, USA, 2016.
24. National Institute for Occupational Safety and Health (NIOSH). Method 7402: Asbestos by TEM. In *NIOSH Manual of Analytical Methods*, 5th ed.; National Institute for Occupational Safety and Health (NIOSH): Washington, DC, USA, 2016.
25. Verein Deutscher Ingenieure (VDI). *VDI-Richtlinie 3492—Indoor Air Measurement—Ambient Air Measurement—Measurement of Inorganic Fibrous Particles—Scanning Electron Microscopy Method*; VDI/DIN-Kommission Reinhaltung der Luft (KRdL)—Normenausschuss: Düsseldorf, Germany, 2013.
26. Deutsche Gesetzliche Unfallversicherung (DGUV). *Method for the Separate Determination of Concentrations of Inorganic Fibres in Work Areas—Scanning Electron Microscopic Method*; DGUV Information 213-546 (former BGI 505-46); Deutsche Gesetzliche Unfallversicherung (DGUV): Berlin, Germany, 2014.
27. German Committee on Hazardous Substances (AGS). *TRGS 402: Identification and Assessment of the Risks from Activities Involving Hazardous Substances: Inhalation Exposure*; Gemeinsames Ministerialblatt: Hürth, Germany, 2010; pp. 231–253.
28. German Committee on Hazardous Substances (AGS). *TRGS 519: Asbestos: Demolition, Reconstruction or Maintenance Work*; Gemeinsames Ministerialblatt: Hürth, Germany, 2014; pp. 164–201.
29. German Committee on Hazardous Substances (AGS). *TRGS 517: Activities with Potentially Asbestos-Containing Minerals and Mixtures and Products Manufactured from Same*; Gemeinsames Ministerialblatt: Hürth, Germany, 2013; pp. 382–396.
30. Fortini, R.; Meyer-Plath, A.; Kehren, D.; Gernert, U.; Jácome, L.A.; Sturm, H. Measurement of flexural rigidity of multi-walled carbon nanotubes by dynamic scanning electron microscopy. *Fibers* **2020**, *8*, 31. [[CrossRef](#)]
31. Nagai, H.; Okazaki, Y.; Chew, S.H.; Misawa, N.; Yamashita, Y.; Akatsuka, S.; Ishihara, T.; Yoshikawa, Y.; Yasui, H.; Jiang, L.; et al. Diameter and rigidity of multiwalled carbon nanotubes are critical factors in mesothelial injury and carcinogenesis. *Proc. Natl. Acad. Sci. USA* **2011**, *108*, E1330–E1338. [[CrossRef](#)] [[PubMed](#)]
32. Gebel, T. Small difference in carcinogenic potency between GBP nanomaterials and GBP micromaterials. *Arch. Toxicol.* **2012**, *86*, 995–1007. [[CrossRef](#)] [[PubMed](#)]
33. Broßell, D.; Heunisch, E.; Meyer-Plath, A.; Bäger, D.; Bachmann, V.; Kämpf, K.; Dziurawitz, N.; Thim, C.; Wenzlaff, D.; Schumann, J.; et al. Assessment of nanofibre dustiness by means of vibro-fluidization. *Powder Technol.* **2019**, *342*, 491–508. [[CrossRef](#)]
34. Moré, J.; Dziurawitz, N.; Thim, C.; Hemmleb, M.; Berger, D. Relocation of defined sample positions with an automated stage navigation tool for SEM. In *Proceedings of the Microscopy Conference 2017, Lausanne, Switzerland, 21–25 August 2017*.
35. Frei, M.; Kruis, F. FibeR-CNN: Expanding Mask R-CNN to improve image-based fiber analysis. *Powder Technol.* **2021**, *377*, 974–991. [[CrossRef](#)]
36. Schumann, J.; Kämpf, K.; Meyer-Plath, A.; Plitzko, S. Automated detection, tracking and characterization of toxicologically relevant nanoscale fibres in scanning electron microscope images. In *Proceedings of the IEEE International Symposium on Biomedical Imaging (ISBI), Venice, Italy, 8–11 April 2019*.
37. Bäger, D.; Plitzko, S.; Broßell, D.; Dziurawitz, N.; Thim, C.; Wenzlaff, D.; Hutsch, T.; Weißgärber, T. Anwendungssichere nanokohlenstoffbasierte Fasermaterialien. *Gefahrst. Reinhalt. Luft* **2020**, *80*, 257–265.
38. Asbach, C.; Kaminski, H.; Von Barany, D.; Kuhlbusch, T.A.J.; Monz, C.; Dziurawitz, N.; Pelzer, J.; Vossen, K.; Berlin, K.; Dietrich, S.; et al. Comparability of Portable Nanoparticle Exposure Monitors. *Ann. Occup. Hyg.* **2012**, *56*, 606–621. [[CrossRef](#)]
39. Asbach, C.; Alexander, C.; Clavaguera, S.; Dahmann, D.; Dozol, H.; Faure, B.; Fierz, M.; Fontana, L.; Iavicoli, I.; Kaminski, H.; et al. Review of measurement techniques and methods for assessing personal exposure to airborne nanomaterials in workplaces. *Sci. Total Environ.* **2017**, *603–604*, 793–806. [[CrossRef](#)]
40. Kehren, D.; Simonow, B.; Bäger, D.; Dziurawitz, N.; Wenzlaff, D.; Thim, C.; Neuhoﬀ, J.; Meyer-Plath, A.; Plitzko, S. Release of respirable fibrous dust from carbon fibers due to splitting along the fiber axis. *Aerosol Air Qual. Res.* **2019**, *19*, 2185–2195. [[CrossRef](#)]

41. British Standards Institution (BSI). *Workplace Exposure. Measurement of Exposure by Inhalation to Chemical Agents. Strategy for Testing Compliance with Occupational Exposure Limit Values*; BS EN 689:2018; British Standards Institution (BSI): London, UK, 2018.
42. Plitzko, S.; Meyer-Plath, A.; Dziurawicz, N.; Simonow, B.; Steinle, P.; Mattenklott, M. Messung nano- und mikroskaliger faserförmiger Materialien an Arbeitsplätzen—Teil 2. *Gefahrst. Reinhalt. Luft* **2018**, *78*, 251–256.
43. Olive, K.A. Section 39. 4.2.3 of review of particle physics. In *Chinese Physics C*; IOP Publishing: Bristol, UK, 2016; Volume 40, p. 100001.
44. Patil, V.V.; Kulkarni, H.V. Comparison of confidence intervals for the Poisson mean: Some new aspects. *REVSTAT—Stat. J.* **2012**, *10*, 211–227.
45. Cousins, R.D. Why isn't every physicist a Bayesian? *Am. J. Phys.* **1995**, *63*, 398–410. [[CrossRef](#)]
46. Bitjukov, S.; Medvedev, V.; Smirnova, V.; Zernii, Y. Experimental test of the probability density function of true value of Poisson distribution parameter by single observation of number of events. *Nucl. Instrum. Methods Phys. Res. Sect. A* **2004**, *534*, 228–231. [[CrossRef](#)]
47. Bitjukov, S.I.; Krasnikov, N.V.; Taperechkina, V.A. Confidence intervals for poisson distribution parameter. *arXiv* **2001**, arXiv:0108020.

Publisher's Note: MDPI stays neutral with regard to jurisdictional claims in published maps and institutional affiliations.



© 2020 by the authors. Licensee MDPI, Basel, Switzerland. This article is an open access article distributed under the terms and conditions of the Creative Commons Attribution (CC BY) license (<http://creativecommons.org/licenses/by/4.0/>).